Title

PKMYT1 Is a Marker of Treatment Response and a Therapeutic Target for CDK4/6 Inhibitor-Resistance in ER+ Breast Cancer.

Journal

Molecular Cancer Therapeutics, 23(10)

Authors

Chen, Anran
Kim, Beom-Jun
Mitra, Aparna
et al.

Publication Date

2024-10-01

DOI

10.1158/1535-7163.MCT-23-0564

Peer reviewed

PKMYT1 Is a Marker of Treatment Response and a Therapeutic Target for CDK4/6 Inhibitor-Resistance in ER$^+$ Breast Cancer

Anran Chen[1,2,3], Beom-Jun Kim[1,4], Aparna Mitra[1], Craig T. Vollert[1,5], Jonathan T. Lei[1,6], Diana Fandino[1], Meenakshi Anurag[1,7,8], Matthew V. Holt[1], Xuxu Gou[1], Jacob B. Pilcher[1], Matthew P. Goetz[9], Donald W. Northfelt[10], Susan G. Hilsenbeck[1,8], C. Gary Marshall[3], Marc L. Hyer[3], Robert Papp[11], Shou-Yun Yin[11], Carmine De Angelis[12], Rachel Schiff[1,4,7,8], Suzanne A.W. Fuqua[1,4,8], Cynthia X. Ma[13], Charles E. Foulds[1,7,8], and Matthew J. Ellis[1,8]

ABSTRACT

Endocrine therapies (ET) with cyclin-dependent kinase 4/6 (CDK4/6) inhibition are the standard treatment for estrogen receptor-α-positive (ER$^+$) breast cancer, however drug resistance is common. In this study, proteogenomic analyses of patient-derived xenografts (PDXs) from patients with 22 ER$^+$ breast cancer demonstrated that protein kinase, membrane-associated tyrosine/threonine one (PKMYT1), a WEE1 homolog, is estradiol (E2) regulated in E2-dependent PDXs and constitutively expressed when growth is E2-independent. In clinical samples, high *PKMYT1* mRNA levels associated with resistance to both ET and CDK4/6 inhibition. The PKMYT1 inhibitor lunresertib (RP-6306) with gemcitabine selectively and synergistically reduced the viability of ET and palbociclib-resistant ER$^+$ breast cancer cells without functional p53. *In vitro* the combination increased DNA damage and apoptosis. In palbociclib-resistant, *TP53* mutant PDX-derived organoids and PDXs, RP-6306 with low-dose gemcitabine induced greater tumor volume reduction compared to treatment with either single agent. Our study demonstrates the clinical potential of RP-6306 in combination with gemcitabine for ET and CDK4/6 inhibitor resistant *TP53* mutant ER$^+$ breast cancer.

Introduction

Most breast cancer-related deaths occur in the setting of ER$^+$ disease (1). Endocrine therapies (ET), in combination with cyclin-dependent kinase 4/6 (CDK4/6) inhibitors (CDK4/6i), such as palbociclib, abemaciclib, or ribociclib, are standard treatments for both high-risk early-stage and/or advanced ER$^+$ breast cancer. Although approximately 80% of ER$^+$ breast cancers initially respond, resistance often develops, leading to treatment refractory and lethal disseminated disease (2). Currently, there is no consensus on the optimal treatment for patients with ET and CDK4/6i-resistant stage 4 disease. Chemotherapy is commonly used but efficacy is limited (3–6).

ATP-dependent protein kinases are aberrantly expressed in cancer and are a critical class of therapeutic target, but only a very small fraction of the more than 500 kinases encoded by the human genome have been successfully targeted (7, 8). Kinase inhibitor pulldown assay (KIPA) offers a sensitive assay to quantify potentially targetable kinases despite low abundance (9–11). However, despite using KIPA technology to identify therapeutic targets in ER$^+$ and triple-negative breast cancer (TNBC; refs. 9, 10, 12), KIPA technology has not been applied to the identification of druggable kinases in the setting of ET and CDK4/6i resistance in ER$^+$ breast cancer.

Herein, we applied a KIPA assay to investigate ET and CDK4/6i resistance in ER$^+$ breast cancers by analyzing 22 distinct ER$^+$ patient-derived xenografts (PDXs) that displayed varying degrees of estradiol (E2) dependence for growth *in vivo*. We identified that the levels of the WEE1 homolog and G2/M cell cycle checkpoint regulatory kinase protein kinase, membrane-associated tyrosine/

[1]Lester and Sue Smith Breast Center, Baylor College of Medicine, Houston, Texas. [2]Integrative Molecular and Biomedical Sciences Program, Baylor College of Medicine, Houston, Texas. [3]Repare Therapeutics, Cambridge, Massachusetts. [4]Department of Molecular and Cellular Biology, Baylor College of Medicine, Houston, Texas. [5]Employee of Adrienne Helis Malvin Medical Research Foundation, New Orleans, Louisiana. [6]Department of Human and Molecular Genetics, Baylor College of Medicine, Houston, Texas. [7]Department of Medicine, Baylor College of Medicine, Houston, Texas. [8]Dan L Duncan Comprehensive Cancer Center, Baylor College of Medicine, Houston, Texas. [9]Department of Oncology, Mayo Clinic, Rochester, Minnesota. [10]Division of Hematology and Medical Oncology at Mayo Clinic, Phoenix, Arizona. [11]Repare Therapeutics, Saint-Laurent, Quebec, Canada. [12]Department of Clinical Medicine and Surgery, University of Naples Federico II, Naples, Italy. [13]Division of Oncology, Department of Internal Medicine, Washington University School of Medicine, St. Louis, Missouri.

Current address for B.-J. Kim: AstraZeneca, Gaithersburg, Maryland; and current address for X. Gou, CSF Helen Diller Family Comprehensive Cancer Center, University of California San Francisco, San Francisco, California.

A. Mitra and C.T. Vollert contributed equally to this article.

Corresponding Authors: Matthew J. Ellis, Progendis Inc., 2429 Bissonnet Street, Suite 531, Houston, TX 77005. E-mail: matthew.ellis@progendis.com; and Charles E. Foulds, Baylor College of Medicine, One Baylor Plaza, ABBR Building, Room R517, Houston, TX 77030. E-mail: foulds@bcm.edu

Mol Cancer Ther 2024;23:1494–510

doi: 10.1158/1535-7163.MCT-23-0564

threonine one (PKMYT1) were highly E2 regulated in E2-dependent PDX models. In contrast, PKMYT1 levels were constitutively high in E2-independent ER+ PDX models and associated with an elevated E2F transcriptional signature, implying G1/S cell cycle deregulation. We therefore sought to study the functional role of PKMYT1 in ER+ breast cancer through correlation with survival in published molecularly characterized breast cancer datasets; to investigate relationships between *PKMYT1* mRNA levels and response to preoperative treatment to both aromatase inhibitor (AI) and palbociclib; and to establish the therapeutic potential of the clinical grade PKMYT1 inhibitor lunresertib (RP-6306; ref. 13) in combination with the nucleoside analog gemcitabine in a spectrum of preclinical models of ER+ breast cancer including cell lines, PDX-derived organoids, and *in vivo* PDX tumors.

Materials and Methods

PDX and clinical data analysis

Proteogenomic data associated with 22 ER+ breast cancers have been reported by Gou and colleagues (9). The raw mass spectrometry (MS) and sequencing read data are available from PRIDE and dbGaP as cited below. In the KIPA analysis, for each kinase, the not available (NA) values were converted to the minimum detected kinase level across the samples – 1.

Data from the METABRIC cohort (14, 15) were obtained from the cBioPortal for Cancer Genomics (cbioportal.org; RRID: SCR_014555), and data from the Clinical Proteomic Tumor Analysis Consortium (CPTAC) breast cancer prospective cohort (16) were obtained from LinkedOmics (linkedomics.org). Z1031B data were obtained from ref. 4, and NeoPalAna data were obtained from ref. 17.

The single-sample gene set enrichment analysis (ssGSEA) scores were computed with mRNA from 22 ER+ PDX tumors and NeoPalAna trial patients using "h.all.v7.0.symbols.gmt" database and default parameters for the R gui implementation of ssGSEA2.0 (GitHub, RRID:SCR_002630; https://github.com/broadinstitute/ssGSEA2.0). RNA-based multigene proliferation scores (MGPS) were calculated as described previously (4) by averaging the gene median-centered $\log_2$ RSEM data for genes previously characterized as cycle-regulated (18).

Cell culture

MCF7 (ATCC Cat. # HTB-22, RRID:CVCL_0031) and T47D (ATCC Cat. # HTB-133, RRID:CVCL_0553) lines were obtained via the Tissue Culture Core at BCM in 2017 from the ATCC, with validation by short tandem repeat (STR) testing completed at the Cytogenetics and Cell Authentication Core (CCAC) at MD Anderson. T47D and MCF7 estrogen-deprivation resistant (EDR) parental lines and their Palbo-R derivatives were described previously (19, 20) and were validated by STR testing completed at CCAC. Cells were cultured at 37°C in 5% CO_2 and were tested for mycoplasma every 6 months. Cell lines were passaged at most 10 to 20 times.

MCF7 and T47D cells were maintained in RPMI 1640 media with 10% FBS (Sigma; cat. # F0926), 1% penicillin-streptomycin (Sigma; cat. # P4333), and 5 μg/mL Plasmocin Prophylactic (InvivoGen; cat. # ant-mpp). MCF7 EDR and MCF7 EDR Palbo-R cells were maintained in phenol red–free RPMI 1640 with 10% charcoal-stripped FBS (Sigma; cat. # F6765), 1% penicillin-streptomycin, and 5 μg/mL Plasmocin. The Palbo-R cell lines were maintained in 1 μmol/L palbociclib.

For treatment experiments, the antibiotics and drugs for maintenance were removed. RPMI 1640 media with 10% FBS were used for MCF7 and T47D cells (parental and Palbo-R), and phenol red–free RPMI 1640 with 10% charcoal-stripped FBS were used for MCF7 EDR and MCF7 EDR Palbo-R, unless otherwise specified. If the treatment reagents were dissolved in DMSO [fulvestrant, palbociclib, abemaciclib, ribociclib, RP-6306, 5-fluorouracil (5-FU), and bortezomib], the same concentration of DMSO was added to the vehicle control as well as other samples without DMSO-based drug solutions.

In experiments involving response to E2, the cells were first cultured in phenol red–free RPMI 1640 with 10% charcoal-stripped FBS for 3 days and then treated with phenol red–free RPMI 1640 with 10% charcoal-stripped FBS containing E2 (and other ligands).

Chemical reagents

E2 was used either in a water-soluble form (Sigma; cat. # E4389) or dissolved in ethanol (Sigma; cat. # E8875) and stored as 10 mmol/L solutions at −80°C. Fulvestrant was from MedChem Express (cat. # HY-13636) and stored as 10 mmol/L solution in DMSO at −20°C. Palbociclib was from Selleckchem (cat. # S4482) and stored as 10 mmol/L solution in DMSO at −20°C. Abemaciclib was from Selleckchem (cat. # S5716) and stored as 5 mmol/L solution in DMSO at −20°C. Ribociclib was from Selleckchem (cat. # S7440) and stored as 10 mmol/L solution in DMSO at −20°C. AZD1775 was from Selleckchem (cat. # S1525) and stored as 10 mmol/L solution in DMSO at −80°C. Gemcitabine was from Sigma (cat. # 1288463) and stored as a 10 mmol/L solution in water at −80°C. RP-6306 was provided by Repare Therapeutics as a 10 mmol/L solution in DMSO and stored at −20°C or as a powder for making drug chow pellets for PDX *in vivo* experiments. Repare Therapeutics has published a detailed schema for how RP-6306 was made (21). Gemcitabine (Cayman; cat. # 11690) for animal injection was dissolved in preservative-free 0.9% sodium chloride (Hospira) on the day of injection. Bortezomib was from Cell Signaling Technology (CST; cat. # 2204S) and stored as a 1 mmol/L solution in DMSO at −20°C. 5-FU was from Selleckchem (cat. # S1209) and stored as a 10 mmol/L solution in DMSO at −80°C.

Reverse transcription–quantitative PCR

RNA was isolated using the RNeasy Mini Kit (QIAGEN; cat. # 74106) with concentration determined using a NanoDrop spectrophotometer. One-step RT-qPCR was conducted using 50 ng RNA incubated with SsoAdvanced Universal SYBR Green Supermix (Bio-Rad; cat. # 1725274), iScript reverse transcriptase (Bio-Rad; cat. # 170-8891) and 0.5 μmol/L primers as described previously (22). Primer sequences for *GAPDH* and *TFF1* were previously described (22). Other primer sequences are listed here: *PKMYT1*: Forward, 5′-GTGAGGTCCAGGAGGGAGA-3′, Reverse, 5′-CACTTCCAGGATGGTGAGG-3′. *CDK6*: Forward, 5′-TCGATGAACTAGGCAAAGACC-3′; Reverse, 5′-AGGTGGGAATCCAGGTTTTC-3′; *RB1*: Forward, 5′- CTGTCTGAGCACCCAGAATTAG -3′; Reverse, 5′- GTCCAAATGCCTGTCTCTCAT-3′; *CDK1*: Forward, 5′- ACAAAGGAACAATTAAACTGGCTG-3′; Reverse, 5′- CTGGAGTTGAGTAACGAGCTG-3′. All samples were run in triplicate on a CFX96 thermal cycler (Bio-Rad).

Immunoblotting

Cell lysates were prepared in RIPA buffer (Thermo Scientific; cat. # 89900) supplemented with protease and phosphatase inhibitors (Roche; SKU 4906845001 and SKU 11697498001, respectively).

Animal tissue lysates were prepared in 8 mol/L urea with sonication. Proteins were separated by SDS-PAGE on gradient gels (4%–15%; Invitrogen; cat. # NW04120BOX, NW04122BOX, NW04125BOX, and NW04127BOX) and transferred to nitrocellulose membranes (Bio-Rad; cat. # 1620115). Anti-CDK1 pT14 (cat. # 2543, RRID:AB_823465), γH2AX (cat. # 9718, RRID:AB_2118009), RB1 (cat. # 9309, RRID:AB_823629), mouse anti-RB1 (cat. # 9313, RRID:AB_1904119), RB1 pS780 (cat. # 8180, RRID:AB_10950972), p53 (cat. # 9282, RRID:AB_331476), ATR pY1989 (cat. # 30632, RRID:AB_2798992), PARP1 (cat. # 9542, RRID:AB_2160739), cleaved PARP1 (cat. # 9541, RRID:AB_331426), Caspase 3 (cat. # 9662, RRID:AB_331439), cleaved Caspase 3 (cat. # 9661, RRID:AB_2341188), and Cyclin E1 (cat. # 20808, RRID:AB_2783554) primary antibodies, and anti-rabbit and mouse (cat. # 7074, RRID:AB_2099233 and cat. # 7076, RRID:AB_330924, respectively) secondary ECL-conjugated antibodies were from CST. Anti-PKMYT1 (cat. # A302-424A, RRID:AB_1907307) primary antibody was from Bethyl Laboratory. Anti-total CDK1 (cat. # 33-1800, RRID:AB_2533105) and anti-total ATR (cat. # PA5-17265, RRID:AB_10975231) primary antibodies were from Thermo Fisher Scientific. Anti-β-actin (cat. # SAB5600204, RRID:AB_3097735) and estrogen receptor-α (cat. # PLA0113, RRID:AB_3097737) primary antibodies were from Sigma. Anti-GAPDH (cat. # sc-32233, RRID:AB_627679) primary antibody was from Santa Cruz Biotechnology. Signals were produced by ECL Select Western Blotting Detection Reagent (Cytiva # RPN2235) and detected by ChemiDoc Touch Imaging System (Bio-Rad).

Immunoblot band intensities were quantified by ImageJ (RRID:SCR_003070; ref. 23). Empty regions above or below target bands were used as the background. CDK1 pT14 and ATR pY1989 signal intensities were normalized by total CDK1 and ATR, respectively. All other proteins were normalized by GAPDH.

Lentiviral production and selection

HEK 293T/17 cells (ATCC; cat. # CRL-3216, RRID:CVCL_0063) were transfected with short hairpin RNA (shRNA) or *PKMYT1* promoter plasmids (described below) together with the packaging plasmids pMD2.G (gift from Didier Trono; Addgene plasmid, # 12259; RRID:Addgene_12259) and psPAX2 (gift from Didier Trono; Addgene plasmid, # 12260; RRID:Addgene_12260) using Lipofectamine 3000 Transfection Reagent (Thermo Fisher Scientific; cat. # L3000001) overnight. The medium was replaced the next day, and the supernatants containing lentiviral particles were harvested every 24 hours for 2 days after transduction. The supernatants were filtered and concentrated by Amicon Ultra-15 centrifugal filter devices (Millipore Sigma; cat. # UFC903024) at 1,000 g for 10 minutes, and stored at −80°C.

Lentiviruses were added to the cells with 6 μg/mL polybrene (Sigma-Aldrich; cat. # 107689) at a multiplicity of infection (MOI) <1. Transduced cells were selected by 1 to 2 μg/mL puromycin (Sigma; cat. # P8833) or 500 μg/mL Geneticin (G418 sulfate; Life Technologies; cat. # 10-131-035) for 1 week until the nontransduced cells were all killed. Cells were maintained after selection in 125 μg/mL G418 and 0.25 to 0.5 μg/mL puromycin before drug studies.

Generation of *PKMYT1* promoter reporter, *TP53* or *RB1* knockdown, and FLAG-tagged wild-type p53 "rescue" cell lines

T47D, T47D Palbo-R, MCF7 EDR, and MCF7 EDR Palbo-R cell lines expressing *Gaussia* luciferase (GLuc) under the control of the human *PKMYT1* promoter were created by lentiviral transduction using a *PKMYT1* promoter-GLuc reporter obtained from GeneCopoeia (cat. # HPRM40000-LvPG04).

For lentiviral transduction of MCF7 EDR and MCF EDR Palbo-R cells, nontargeting shRNA and two different *TP53*-targeting shRNAs in the pGIPZ lentiviral vector were obtained from Horizon Discovery (cat. # RHS4346, RHS4430-200296439, and RHS4430-200289946, respectively).

For lentiviral transduction of MCF7 cells, two different *RB1*-targeting shRNAs in the pGIPZ lentiviral vector were obtained from the BCM Advanced Cell Engineering and 3D Models Core (Horizon Discovery sells as cat. # RHS4430-200184904 and RHS4430-200183214, respectively).

For lentiviral transduction of T47D Palbo-R cells to knockdown endogenous mutant *TP53* encoding L194F mutant protein and re-express FLAG-tagged WT p53 protein, cells were first infected with a virus expressing shRNA targeting the 3′ untranslated region (UTR) of mutant *TP53* (Sigma; cat. # TRCN0000010814) or a control non-targeting shRNA (Sigma; cat. # SHC016) and then selected with puromycin as indicated. Stable cells were then transduced with a virus expressing either N-terminal FLAG-tagged WT p53 without its 3′ UTR (GeneCopoeia; cat. # EX-B0105-Lv101) or N-terminal FLAG-tagged EGFP (GeneCopoeia; cat. # EX-EGFP-Lv101) as a control, followed by G418 selection as indicated.

PKMYT1 promoter assay

Promoter activity in *PKMYT1* promoter reporter cell lines were measured by the activity of *Gaussia* luciferase (GLuc) whose transcription was under the control of a 1.3 kb sequence upstream of the *PKMYT1* transcription start site. Cells were treated with 1 μmol/L of palbociclib or DMSO for 2 days. The media from both groups were refreshed after day 1. The day 2 supernatant media was used to measure GLuc activity. Within each treatment, the GLuc activity was normalized by the activity of CMV promoter-expressed secreted alkaline phosphatase (SEAP) that was present in the lentiviral vector. Supernatant from nontransduced cells were used for measuring background luminescence. Reagents for measuring GLuc and SEAP activities were from Secrete-Pair *Gaussia* Luciferase Assay Kit (GeneCopoeia; cat. # LF062). In this kit, buffer GL-H was used for measuring GLuc activities.

KIPA-SureQuant for targeted kinase level determination in T47D parental and T47D Palbo-R cells

We previously described a targeted quantification method (called "SureQuant") for absolute level detection of 106 kinase peptides by spike-in of heavy labeled synthetic peptides after KIPA was performed (11). We used this assay platform to interrogate T47D parental versus T47D Palbo-R cells and determined steady-state levels for 81 kinases as shown in Supplementary Table S1.

Cell growth assays

Cells of interest were plated in 96 well plates with a density of 500 to 1,000 cells/well 1 day before the drug treatment. Existing media was replaced with fresh media with drugs on days 2 or 3. Viability was measured on day 6 by an alamarBlue assay (Invitrogen; cat. # DAL1100) as described previously (22).

Drug synergy and sensitivity analysis

Dose–response curves were simulated using R package drc (3.0-1) with the three-parameter log-logistic function (LL.3). Loewe synergy scores and combination sensitivity scores were calculated by R package SynergyFinder (3.2.10, RRID:SCR_019318; 24). Synergy

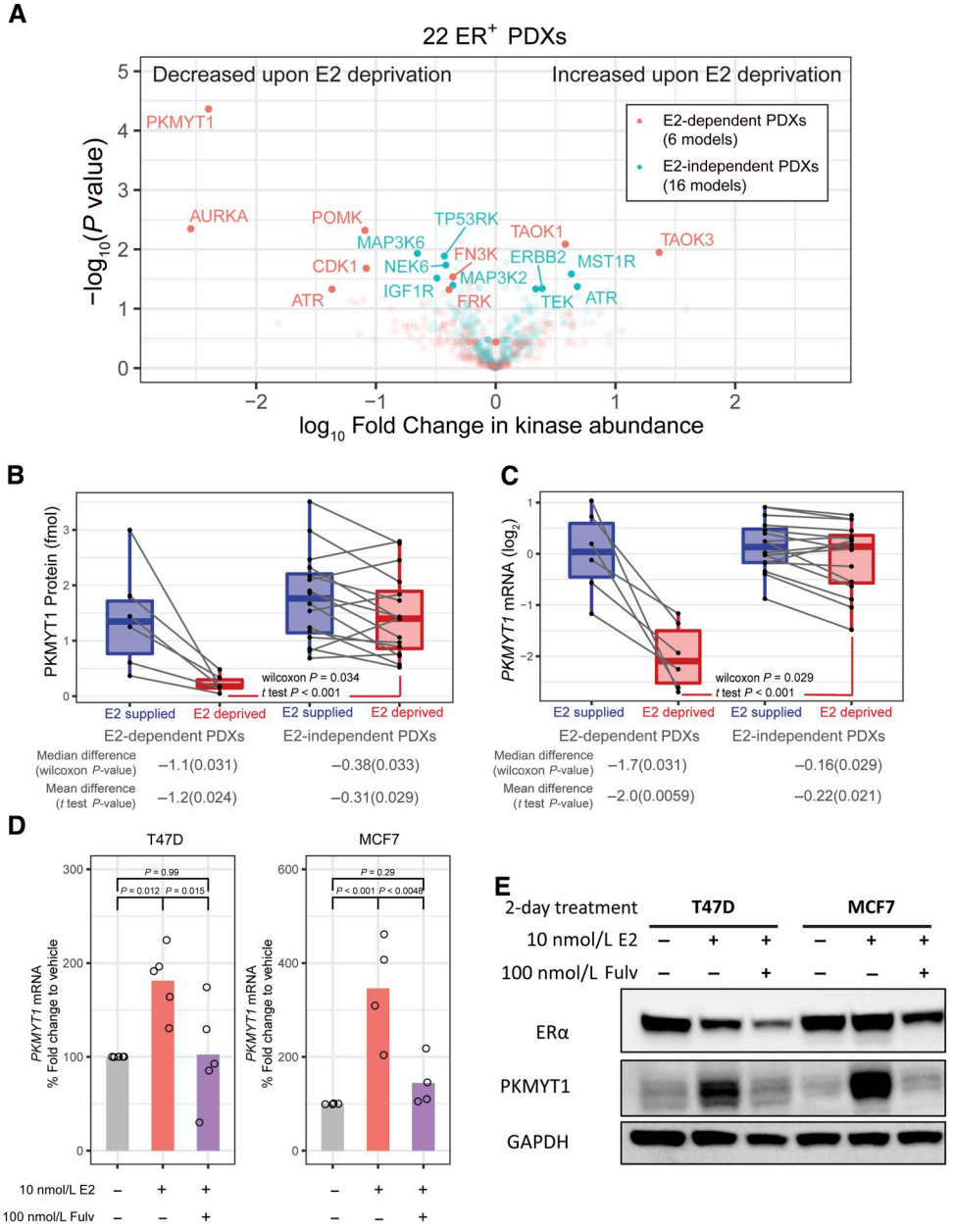

Figure 1.

PKMYT1 mRNA and protein levels are E2-regulated in ER+ breast cancer PDXs and cell lines. **A,** Volcano plot showing the effect of E2-deprivation on kinase levels in 22 ER+ PDXs whose tumor growth was either E2-dependent or E2 independent. All mice were ovariectomized before exogenous E2 was supplied or not. Levels were determined by KIPA. Differentially expressed kinases with *P*-values < 0.05 are labeled. **B,** Absolute PKMYT1 protein levels in individual PDX lines were measured by KIPA-SureQuant. **C,** *PKMYT1* mRNA levels in individual PDX lines were determined by RNA-seq. **D,** RT-qPCR of *PKMYT1* mRNA in hormone-deprived MCF7 and T47D cells treated with vehicle, 10 nmol/L E2, and E2 with 100 nmol/L fulvestrant for 2 days. **E,** Immunoblotting of protein lysates from hormone-deprived MCF7 and T47D cells treated with vehicle, 10 nmol/L E2, and E2 with 100 nmol/L fulvestrant for 2 days. ERα was decreased by fulvestrant as expected. GAPDH serves as a loading control. The figure is a representative image of three independent biological replicates. In (**A**), *P*-values were calculated by paired *t* test. In (**B**) and (**C**), Wilcoxon signed-rank test *P*-values were shown after the median difference; paired *t* test *P*-values were shown after the mean difference. Wilcoxon rank sum test and *t* test were used to compare E2-deprived samples. In (**D**), bars show the means of individual biological repeats indicated by the dots. *P*-values were calculated with one-way ANOVA and Tukey HSD.

scores between cell lines were compared using Wilcoxon signed-rank test. Combination viability was calculated by subtracting 100 by the combination sensitivity score. Approximate *P*-values of the combination viability comparison were determined by *z*-tests using the combination viability and the standard error of mean (SEM) of the models.

Cell death assays

Cells of interest were plated in 96-well plates with a density of 5,000 cells/well 1 day before the drug treatment. Dead cells were labeled by CellTox Green Cytotoxicity Assay (Promega; cat. # G8741) by adding it to the media at the beginning of the treatment at a 1:1,000 ratio. Cells were imaged at the phase and GFP channels 3 days after the treatment started. Images were taken by Essen Incucyte ZOOM (RRID:SCR_019874). The numbers of green objects, which indicate the dead cells, were quantified by Incucyte ZOOM 2018A software.

PDX organoids and *in vivo* drug testing

The ER+ PDX models were previously described (9). All animal procedures were approved by the Institutional Animal Care and Use Committee at BCM (protocol AN-6934).

PDX organoids

The establishment of PDX organoid (PDxO) from PDX single-cell suspensions and the growth media for PDxO have been previously described (9). Organoids were plated on 96-well plates and treated for 2 weeks with a media/drug change every 3 or 4 days. To

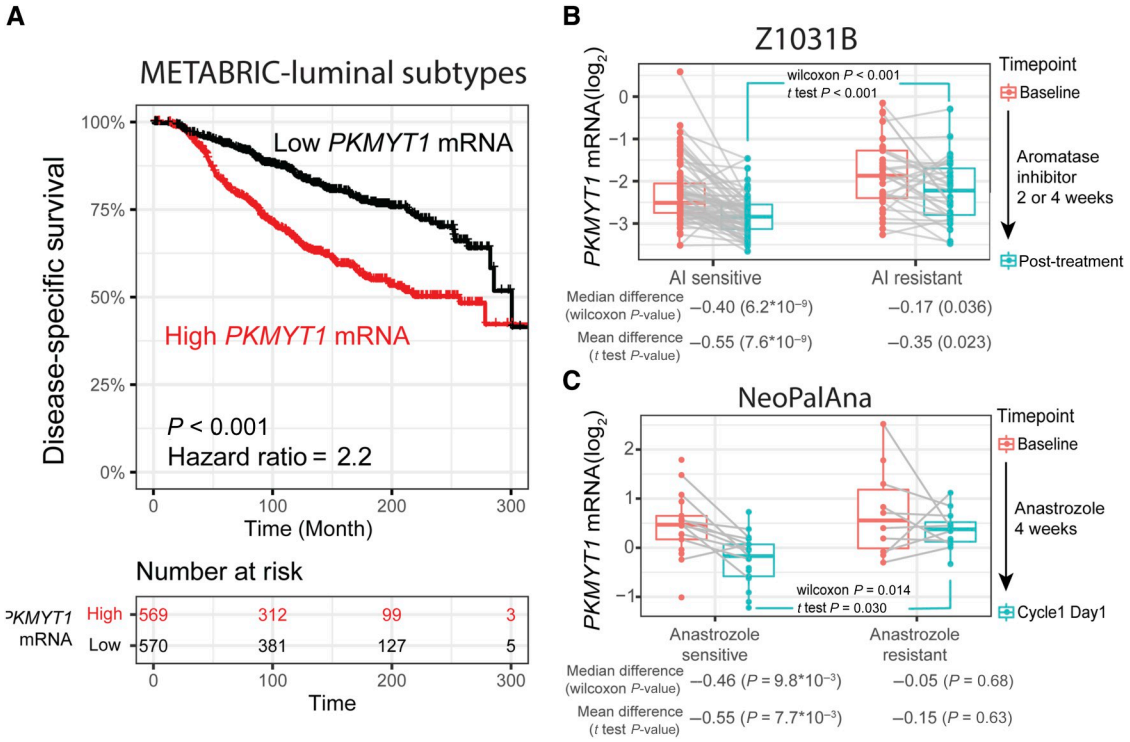

Figure 2.

PKMYT1 mRNA levels are significantly associated with patient outcome and endocrine therapy response. **A,** Kaplan–Meier survival curves of disease-specific survival of patients with Luminal A and B (ER^+) breast cancer in the METABRIC cohort, stratified by the median of *PKMYT1* mRNA. Numbers of patients with high or low *PKMYT1* mRNA are shown at the bottom. **B,** *PKMYT1* mRNA level of pre- and post- AI treatment tumors of the patients from the ACOSOG Z1031B trial, grouped by AI clinical response (AI sensitive or AI resistant). **C,** *PKMYT1* mRNA level of pre- and post-anastrozole treatment tumors of the patients from the NeoPalAna trial, grouped by anastrozole clinical response. In (**A**), the *P*-value and hazard ratio were calculated by the Cox Proportional-Hazards model. In (**B** and **C**), Wilcoxon signed-rank test *P*-values were shown after the median difference; paired *t* test *P*-values were shown after the mean difference. Wilcoxon rank sum test and *t* test were used to compare E2 post-treatment samples.

measure viability after 2 weeks, the media was removed. Organoids were digested using 50 µL 1 U/mL dispase (STEMCELL Technologies; cat. # 07923) for 45 minutes at 37°C. 70 µL CellTiter-Glo 3D reagent (Promega; cat. # G9682) was then added and the 96-plates covered by aluminum foil were placed on a shaker at 225 rpm for 20 minutes at room temperature. The mixtures were transferred to opaque 96-well plates to measure luminescence on a BMG luminometer.

In vivo drug testing

Two- to three-mm pieces from BCM-7441 PDX tumors were engrafted into cleared mammary fat pads of 3- to 4-week-old SCID/beige (strain C.B-17/IcrHsd-*Prkdc*^{scid}Lyst$^{bg\text{-}J}$) mice (Envigo). Mice were randomized into five groups to receive treatments ($n = 7$–8 per arm). Treatment groups were vehicle, palbociclib (70 mg/kg in chow), RP-6306 (300 ppm in chow), gemcitabine (20 mg/kg in saline, intraperitoneal injection once a week), and the combination of gemcitabine and RP-6306. Saline was given to all mice that were not treated with gemcitabine once a week as the vehicle control. Tumor volumes were measured by a caliper every 3 to 4 days and were calculated by $V = 4/3 \times \pi \times (\text{width}/2)^2 \times (\text{length}/2)$. For tumors too small to be measured by caliper (≤3 mm), the width and length were denoted as 3 mm. Mice were euthanized when tumors reached 1.5 cm^3 or at the study endpoint.

Statistical analysis

Majority of statistical analyses and figures were generated using R (v4.0.4, The R Foundation for Statistical ComputingRRID: SCR_001905). Kaplan–Meier plots are produced with R package survminer [0.4.9, (RRID:SCR_021094). Dose–response curves were simulated using R package drc (3.0-1; ref. 25)]. Loewe synergy scores and combination sensitivity scores were calculated by R package SynergyFinder (3.2.10, RRID:SCR_019318; ref. 24). Dunnett's tests were performed using R package DescTools (0.99.4). PDXs were clustered by Phantasus v1.19.3 (artyomovlab.wustl.edu/phantasus). All experiments were done with biological replicates of three or more. In quantifying experiments, each biological replicate had two to five technical replicates depending on the experiments. Sources of error, statistical methods and tests, and *P*-values are all reported in the figures and/or figure legends. *P*-values <0.05 were considered statistically significant.

Data availability

Raw proteomics or whole exome sequencing/transcriptomics data from $ER\alpha^+$ PDX tumors that were analyzed in this study are available in the ProteomeXchange Consortium (RRID:SCR_004055) via the PRIDE (26) partner repository with the dataset identifier PXD036644 or in the NCBI database of Genotypes and Phenotypes (dbGaP'RRID: SCR_002709) with accession number phs003324.v1.p1.

Raw KIPA-SureQuant data from T47D parental and T47D-PalboR cells (-/+) palbociclib treatment have been deposited to the ProteomeXchange Consortium (RRID:SCR_004055) via the PRIDE (26) partner repository with the dataset identifier PXD050619.

Results

PKMYT1 expression is E2 regulated in ER+ PDX models when tumor growth is E2 dependent, but constitutively overexpressed in PDXs when growth is E2 independent

We have previously described 22 PDXs from patients with ER+ breast cancer grown in ovariectomized SCID/beige mice with or without exogenous supplementation of E2 (9, 27). Among the 22 PDX lines, 6 PDXs were completely E2 dependent, defined as tumor growth only occurring in the presence of E2. The remaining 16 PDXs exhibited a spectrum of E2 independencies, from partial to complete (9, 27). PDX tumors were also subjected to proteogenomic analyses including whole exome sequencing, RNA sequencing (RNA-seq), and TMT-based MS to generate both proteomic and phosphoproteomic profiles (9, 27). Because ATP-dependent protein kinases are critical therapeutic targets, but often challenging to quantify due to their relatively low abundance, we also analyzed the MS-based kinomes of each PDX using a previously described KIPA (9–11). KIPA revealed a set of kinases that demonstrated E2-dependent regulation in E2-dependent versus E2-independent PDXs. Notably, we observed that PKMYT1, a WEE1 homolog (28–30), exhibited the highest E2 regulation among all kinases in the E2-dependent PDXs but the expression was not significantly altered by E2 exposure in the E2-independent PDXs (**Fig. 1A**). To validate the finding that PKMYT1 is E2 regulated, we used an approach whereby a heavy isotope–labeled PKMYT1 peptide was spiked into tumor lysates ["SureQuant" (11)] to accurately quantify PKMYT1 protein levels. In the E2-dependent PDX tumors, PKMYT1 protein was significantly lower under the E2-deprived condition compared to the E2-supplemented condition (**Fig. 1B**). Although a significant difference was also observed in the E2-independent PDX tumors, PKMYT1 levels were decreased by E2 deprivation to a significantly lesser extent. Similarly, we found that *PKMYT1* mRNA was significantly regulated by E2 treatment in E2-dependent PDXs but remained high in E2-independent PDXs without exogenous E2 supplementation (**Fig. 1C**). Interestingly, the level of the previously clinically targeted WEE family kinase, WEE1, was not significantly altered by E2 exposure in E2-dependent PDXs based on KIPA, and the change was reduced compared to PKMYT1 assessed by SureQuant and RNA-seq (Supplementary Fig. S1).

PKMYT1 expression is regulated by E2 in ER+ breast cancer cell lines

Because *PKMYT1* mRNA is E2 regulated in E2-dependent ER+ breast cancer PDXs, we proceeded to verify whether the regulation might be transcriptional via ERα. By analyzing existing chromatin immunoprecipitation-sequencing (ChIP-seq) datasets from the ER+ breast cancer cell line MCF7 using Cistrome DB (31), we observed chromatin occupancy of ERα in two major peaks at approximately 30 and 40 kilobase pairs upstream of the *PKMYT1* gene transcriptional start site (Supplementary Fig. S2). Interestingly, these ERα peaks overlap regions with H3K27 acetylation (H3K27ac) and H3K4 monomethylation (H3K4me1), which is suggestive of potential enhancer function (Supplementary Fig. S2; ref. 32). Because an enhancer can regulate multiple genes within the same chromosomal space, we then assayed the E2 regulation of nine genes on chromosome 16 in proximity to the ERα-binding sites using existing MCF7 transcriptomic data via the Signaling Pathways Project (33). Among the nine genes, only the expression of *PKMYT1* and *PAQR4* mRNAs were significantly upregulated by E2 (Supplementary Table S2). To further verify whether *PKMYT1* is an ERα-regulated gene at the mRNA level, we treated two ER+ breast cancer cell lines, MCF7 and T47D, with E2 and fulvestrant, a selective ER degrader (34). We found that a 2-day exposure to 10 nmol/L E2 significantly induced *PKMYT1* mRNA as compared to vehicle-treated cell lines, while the addition of 100 nmol/L fulvestrant to 10 nmol/L E2 significantly reduced E2-induced mRNA expression (**Fig. 1D**). Consistent with the mRNA data, immunoblotting confirmed that PKMYT1 protein levels were also E2-induced and that E2-mediated induction can be reversed by fulvestrant (**Fig. 1E**). To determine whether the *PKMYT1* E2 induction is simply not secondary to cell cycle transition, we dysregulated the G1/S checkpoint transition in MCF7 cells by depleting RB1 protein with two different targeting shRNAs and then treated cells with E2. Similar to the well-described ERα target gene *TFF1* [previously called *pS2* (35)], *PKMYT1* mRNA expression was stimulated by E2 with a similar fold change, regardless of *RB1* knockdown, while the E2F target gene *CDK1* [previously called *Cdc2* (36)] displayed a decreased E2 induction fold change after RB1 knockdown due to increased basal expression (Supplementary Fig. S3).

High *PKMYT1* mRNA levels are associated with poor survival and reduced response to endocrine therapy in primary ER+ breast cancer treated with neoadjuvant aromatase inhibition

The METABRIC database (14, 15) was used to confirm the previously published findings based on a The Cancer Genome Atlas analysis that *PKMYT1* mRNA levels are associated with poor outcomes in breast cancer (37). In the Prediction Analysis of Microarray 50 (PAM50) subtypes (38) that were Luminal A or B, high *PKMYT1* mRNA levels were significantly associated with poor prognosis (**Fig. 2A**). To verify correlations between *PKMYT1* mRNA levels and response to ET, we reanalyzed our published transcriptomic data from primary ER+ breast cancers treated in the neoadjuvant setting, where samples were taken both before and on an aromatase inhibitor (AI) to determine individual tumor antiproliferative responses to ET. In the ACOSOG Z1031B trial, patients with stage II/III ER+ breast cancer were treated with an AI for 16 to 18 weeks followed by surgery. A biopsy was taken after 4 weeks and if tumor Ki67 levels were >10% positive, patients were offered a switch to neoadjuvant chemotherapy because of evidence for ET resistance and poor prognosis (4). Among the patients who responded to AI, with a decline in the cell cycle biomarker Ki67 <10%, *PKMYT1* mRNA levels decreased significantly after treatment (**Fig. 2B**). Although *PKMYT1* mRNA levels also decreased in the AI-resistant group (4 weeks Ki67 >10%), the post-treatment level was reduced to a lower extent than in the AI-sensitive group. We subsequently performed an analysis of the NeoPalAna trial, where patients were initially treated with the AI anastrozole for 4 weeks, followed by the combination of anastrozole and the CDK4/6i palbociclib for a further 2 weeks (see below for the effect of CDK4/6 on *PKMYT1* expression; ref. 17). Similar to the ACOSOG Z1031 observations, we observed that after 4 weeks of anastrozole treatment, *PKMYT1* mRNA levels were significantly decreased in the AI-sensitive responders (4 week Ki67 <10%), but not in the AI-resistant cases (4 week Ki67 >10%; **Fig. 2C**). Although protein levels were not measured in the NeoPalAna cohort, we confirmed a significant correlation between PKMYT1 mRNA and protein levels in a

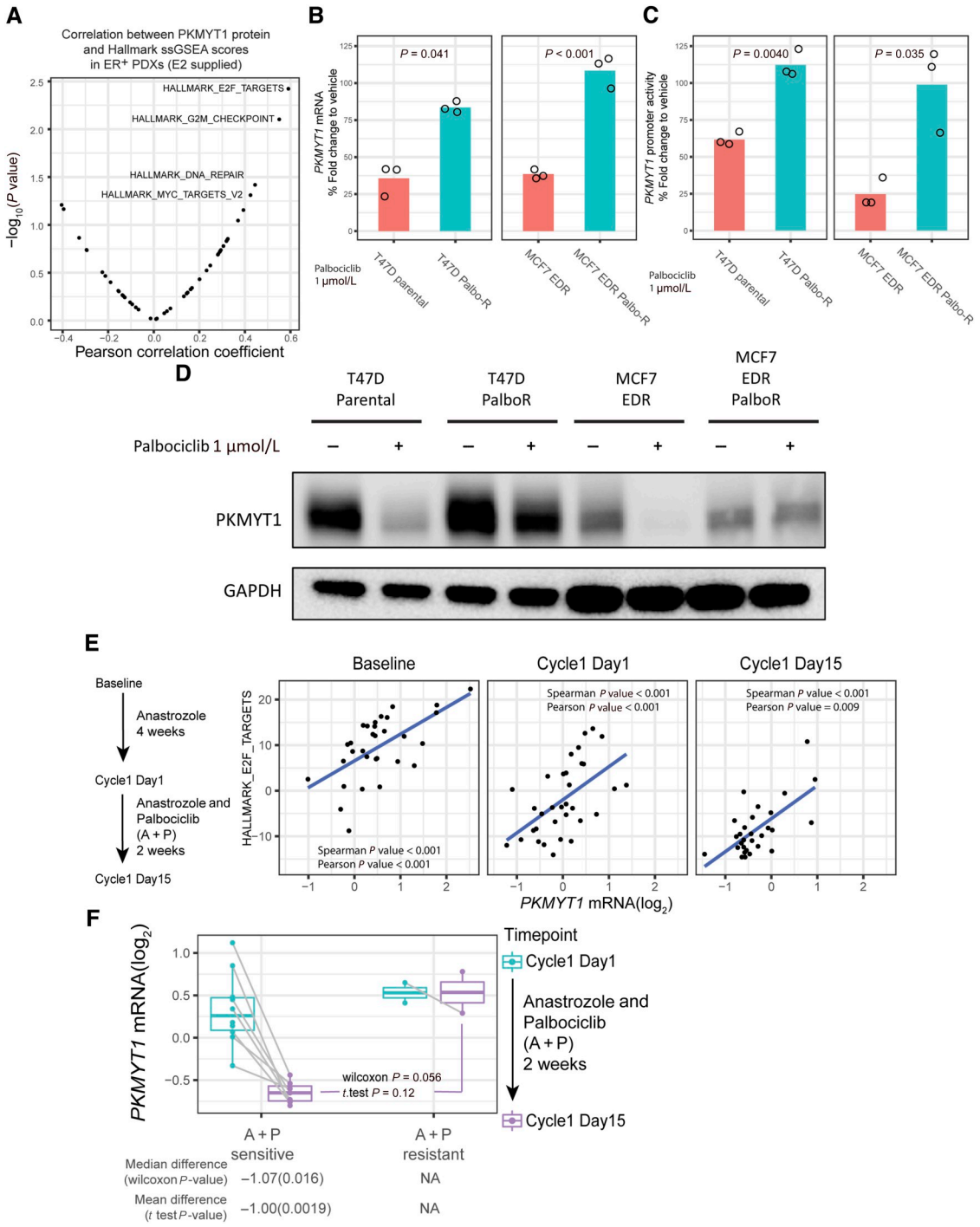

Figure 3.

Expression of PKMYT1 is negatively regulated by palbociclib treatment in sensitive, but not resistant, ER$^+$ breast cancer cell lines and patients. **A,** Volcano plot of the correlation of PKMYT1 protein levels and Hallmark ssGSEA scores in 22 ER$^+$ breast cancer in ovariectomized PDX mice given exogenous E2. Hallmark pathways with *P*-values < 0.05 are labeled. **B,** RT-qPCR of relative *PKMYT1* mRNA level after 1 μmol/L palbociclib treatment for 2 days, adjusted by *GAPDH* mRNA and normalized by the vehicle-treated cells. **C,** Luciferase assays were performed to determine *PKMYT1* promoter activities in cells transduced with a lentivirus-expressing *Gaussia* luciferase (GLuc) under the control of a ~1.3 kb *PKMYT1* promoter (see "Methods"). Cells were treated with 1 μmol/L palbociclib for 2 days, and GLuc values were normalized by the vehicle-treated cells. **D,** Immunoblotting of protein lysates made from cells treated with 1 μmol/L palbociclib or vehicle for 2 days. GAPDH serves as a loading control. The figure is a representative image of three independent biological replicates. **E,** Scatterplots of *PKMYT1* mRNA and Hallmark pathway "E2F Targets" score of NeoPalAna patient samples collected at three stages of treatments [baseline, cycle 1 day 1 (4 weeks (*Continued on the following page.*)

different cohort of samples from patients with luminal breast cancer (the CPTAC breast cancer prospective cohort; ref. 16)] (Supplementary Fig. S4). A similar analysis was conducted on the PKMYT1 homolog *WEE1* since WEE1 inhibitors have been the subject of multiple clinical trials (e.g., ClinicalTrials.gov: NCT03313557 and NCT01748825). Among the patients with luminal breast cancer in the METABRIC cohort, the median *WEE1* mRNA was not prognostic (Supplementary Fig. S5A). The decrease in *WEE1* mRNA with AI was statistically significant but less marked than *PKMYT1* mRNA in ACOSOG Z1031B and was not statistically significant in the NeoPalAna dataset. In both cohorts, no significant difference was observed in the post-treatment *WEE1* mRNA between the responders and the nonresponders. (Supplementary Fig. S5B and S5C). Thus, on the basis of 22 ER+ PDXs and three clinical patient cohorts, our findings suggest that *PKMYT1* is regulated at the mRNA level by E2 and that mRNA levels track with the degree of E2 dependence.

Palbociclib reduces PKMYT1 mRNA and protein levels in palbociclib-sensitive ER+ breast tumors and cell lines

PKMYT1 is a G2/M checkpoint kinase that regulates DNA damage repair through inhibitory phosphorylation of CDK1 (28, 30, 39, 40). To further explore pathways associated with elevated PKMYT1 expression, we analyzed correlations between PKMYT1 protein levels and ssGSEA scores (Supplementary Table S3) among the 22 ER+ PDX tumors under both E2-supplemented and E2-deprived conditions (**Fig. 3A**; Supplementary Fig. S6). As expected, G2M checkpoint and DNA damage repair Hallmark signatures were strongly associated with PKMYT1 protein levels (**Fig. 3A**). Interestingly, the "E2F targets" Hallmark is one of the signatures that are most strongly associated with PKMYT1 protein level, although the *PKMYT1* gene is currently not included in the Hallmark E2F targets in the Molecular Signatures Database (MSigDB) Hallmark gene set (41), indicating that this particular kinase is an underappreciated aspect of E2F-associated biology (**Fig. 3A**; Supplementary Fig. S6). E2F transcription factors are important drivers for G1/S progression in the mammalian cell cycle and these factors are repressed by hypophosphorylated RB1 (42). Cyclin D-CDK4/6 complexes phosphorylate RB1 and inactivate RB1's repression on E2Fs by triggering RB1 dismissal from E2Fs followed by RB1 degradation (43). Clinically, CDK4/6 are important kinase targets in ER+ breast cancer as Cyclin D1 (encoded by *CCND1*) is a well-established ERα target gene that drives cell cycle progression from G1 to S phase (44). There are currently three FDA-approved CDK4/6 inhibitors- palbociclib, abemaciclib, and ribociclib (45–48). On the basis of the above findings, we speculated that *PKMYT1* mRNA levels may also reflect the response to CDK4/6i treatment.

To verify this hypothesis, we used a palbociclib and abemaciclib cross-resistant T47D cell line (termed T47D Palbo-R; ref. 19) and an estrogen deprivation-resistant (EDR) and palbociclib-resistant MCF7 cell line (termed MCF7 EDR Palbo-R; ref. 20), which we demonstrate herein is also abemaciclib and ribociclib resistant (Supplementary Fig. S7). Both CDK4/6i-resistant cell lines were generated by growing parental lines in 1 μmol/L palbociclib for up to 6 months and isolating resistant clones. Importantly, the two cell lines harbor different mechanisms of palbociclib resistance. MCF7 EDR Palbo-R cells have low RB1 levels and overexpressed cyclin E1 (20). In contrast, T47D Palbo-R cells express RB1 and cyclin E1 to similar levels as the parental T47D cells (Supplementary Fig. S8A). However, upon palbociclib treatment, the RB1 phosphorylation is not as strongly inhibited in T47D Palbo-R cells as in T47D parental cells (Supplementary Fig. S8B). We further investigated how T47D-PalboR may be resistant by performing KIPA-SureQuant that employed heavy peptides to 106 kinases (11). In our discovery experiment, we found that CDK6 but not CDK4, had a higher level of expression (~7 fold) in T47D-PalboR versus T47D parental cells (Supplementary Table S1). We further validated that *CDK6* mRNA was overexpressed (~6 fold) in T47D-PalboR versus T47D parental cells (Supplementary Fig. S8C). Our data are consistent with reports that CDK6 overexpression is a mechanism for CDK4/6 inhibitor resistance in ER+ breast cancer cells (49, 50).

Palbociclib-sensitive T47D and MCF7 EDR cell lines and their Palbo-R derivatives were treated with 1 μmol/L palbociclib for 2 days to determine effects on *PKMYT1* mRNA levels. Upon palbociclib treatment, Palbo-R cell lines demonstrated significantly elevated *PKMYT1* mRNA levels as compared to the treated parental cell lines (**Fig. 3B**). In an analysis of published ChIP-seq datasets, we observed that E2F transcription factors (E2F1, E2F4) occupy chromatin near the transcription start site of the *PKMYT1* gene in MCF7 cells (Supplementary Fig. S2; refs. 51, 52). We therefore further tested the effect of palbociclib treatment on *PKMYT1* promoter activity in parental and Palbo-R cells. Cell lines were stably transduced with a *Gaussia* luciferase (GLuc) reporter gene under the control of a 1.3 kb sequence upstream of the *PKMYT1* transcription start site that contains an E2F consensus motif (TTTGGCGC; refs. 53, 54). After a 2-day treatment with 1 μmol/L palbociclib, Palbo-R cell lines demonstrated significantly elevated *PKMYT1* promoter activities, which were determined by GLuc activities, as compared to the treated parental cell lines (**Fig. 3C**). Importantly, PKMYT1 protein levels correlated with mRNA levels and promoter activities in the palbociclib-treated cell lines (**Fig. 3D**).

PKMYT1 mRNA levels are associated with tumor response to palbociclib in clinical trial samples

The association between *PKMYT1* mRNA levels and the tumor response to the CDK4/6i palbociclib was further addressed in the NeoPalAna patient cohort (17). As introduced previously, patients were initially treated with anastrozole for 4 weeks (from baseline to cycle 1 day 1) and then subsequently for 2 weeks with the combination of both anastrozole and palbociclib (denoted as A+P, from cycle 1 day 1 to cycle 1 day 15). The ssGSEA scores were calculated from the mRNA data of tumor samples (Supplementary Table S4). In agreement with the ER+ PDXs findings described above, clinical *PKMYT1* mRNA levels were strongly and significantly associated with the Hallmark E2F targets gene signature throughout the treatment course (**Fig. 3E**). *PKMYT1* mRNA levels in patient samples taken before and after 2 weeks of anastrozole and palbociclib treatment were also analyzed. Among the tumors where Ki67 expression was not suppressed below 10% in response to anastrozole

(*Continued.*) treatment with anastrozole) and cycle 1 day 15 (2 weeks treatment with anastrozole plus palbociclib)]. **F,** *PKMYT1* mRNA level of pre- and post-anastrozole and palbociclib (A+P) treatment tumors of the patients from the NeoPalAna trial who did not initially respond to anastrozole alone, grouped by A+P response. In (**B** and **C**), bars show the means of three individual biological repeats. *P*-values were calculated by *t* test. In (**E**), the trend line was calculated by a linear regression model and *P*-values were calculated by Pearson and Spearman correlation. In (**F**), Wilcoxon signed-rank test *P*-values are shown after the median difference; paired *t* test *P*-values are shown after the mean difference. Wilcoxon rank sum test and *t* test were used to compare E2 post-treatment samples.

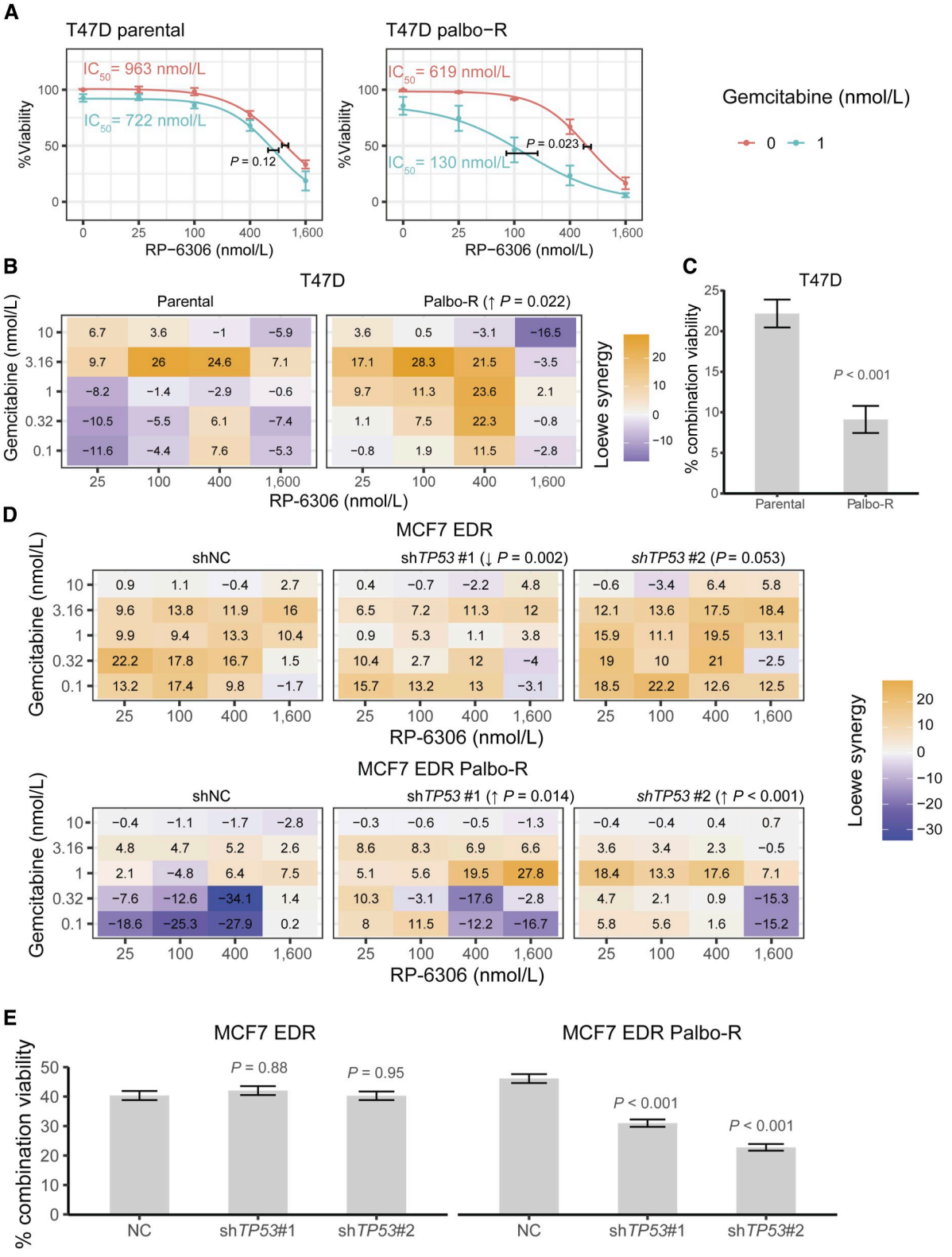

Figure 4.

A clinical-grade PKMYT1 inhibitor (RP-6036) and nucleoside analog (gemcitabine) synergistically and significantly reduce the viability of palbociclib-resistant ER$^+$ breast cancer cells that lack functional p53 protein. **A,** Dose–response curves of RP-6306 effect on the viability of (*Continued on the following page.*)

treatment, most of these tumor samples subsequently exhibited Ki67 suppression after palbociclib treatment. However, there were two nonresponders whose tumors displayed Ki67 >10% after 2 weeks of A+P treatment. In the Ki67 responders (A+P sensitive), *PKMYT1* mRNA levels were significantly decreased by palbociclib. In contrast, the two Ki67-based nonresponders (A+P resistant) exhibited high *PKMYT1* mRNA levels that were unaffected by palbociclib treatment. The difference in post-treatment *PKMYT1* mRNA levels between the Ki67-based responders and nonresponders was on the cusp of statistical significance ($P = 0.056$ by Wilcoxon rank sum test; **Fig. 3F**). Even though the clinical nonresponder number is small, these clinical observations agree with the above preclinical data. Unlike *PKMYT1* mRNA, *WEE1* mRNA levels were not reduced in NeoPalAna patient tumors that were A+P sensitive. Additionally, no significant difference in the post-treatment *WEE1* mRNA levels was observed between the responders and nonresponders (Supplementary Fig. S9). Interestingly, among luminal (ER^+) primary breast tumors in the METABRIC cohort, *PKMYT1* mRNA levels were strongly correlated with *Ki67* mRNA levels (Supplementary Fig. S10).

The combination of a PKMYT1 inhibitor and gemcitabine synergistically reduces the viability of palbociclib-resistant, p53-deficient ER^+ breast cancer cells

As a WEE family kinase, PKMYT1 plays an important role in DNA damage repair coordination at the G2/M checkpoint by preferentially phosphorylating CDK1 at threonine 14 (pT14), a PKMYT1-specific phosphorylation site, unlike tyrosine 15 (pY15), a phosphorylation event catalyzed by WEE1 (13, 30, 39, 40). CDK4/6 inhibitors suppress the growth of sensitive breast cancer cell growth by inducing G1 cell cycle arrest and cellular senescence (55). In ER^+ breast cancer cells resistant to a CDK4/6i, loss of RB1 or overexpression of cyclin E, CDK2, and/or CDK6 can cause G1/S checkpoint bypass (56–59). In this setting, abrogation of the G2/M checkpoint becomes a therapeutic opportunity, since in the absence of a G1/S checkpoint, mitotic catastrophe and cell death can be induced if cells with unrepaired DNA damage from chemotherapy are allowed to enter mitosis (60). Because of the prominent regulation of PKMYT1 in ER^+ breast cancer cells, the possibility of targeting PKMYT1 to increase chemotherapy sensitivity in the setting of combined resistance to both CDK4/6i and ET treatment was explored. RP-6306 is a selective and potent small-molecule PKMYT1 inhibitor in clinical trials (13). Unlike the WEE1 inhibitor AZD1775 (previously named MK1775; ref. 61), RP-6306 selectively binds and inhibits PKMYT1 but not WEE1 in various cancer cell lines and solid tumors (13). As a first step, T47D Palbo-R and its parental cell line were treated with RP-6306 as a single agent, and cell viability was measured after 6 days of treatment. T47D Palbo-R had a lower IC_{50} (616 nmol/L) compared to the parental cells (963 nmol/L), but overall IC_{50}'s were high, indicating low sensitivity (**Fig. 4A**). Importantly, the RP-6306 treatment did not restore the sensitivity of T47D Palbo-R cells to palbociclib (Supplementary Fig. S11). We next tested how the cell line viabilities would be affected by the gemcitabine, a nucleoside analog chemotherapy agent given by intravenous infusion to patients with metastatic ER^+ breast cancer (62), as it was previously shown to synergize with RP-6306 in *CCNE1*-amplified cancer cells (13). Upon exposure to a low dose of the nucleoside analog gemcitabine (1 nmol/L), the IC_{50} of RP-6306 in T47D Palbo-R significantly decreased by approximately five-fold (130 nmol/L), whereas the IC_{50} of RP-6306 in the T47D parental cells remained relatively unaltered (722 nmol/L; **Fig. 4A**). Subsequently, cells were treated with a range of concentrations of RP-6306 and gemcitabine to generate a data matrix for two-drug Loewe synergy scores (24) for synergy and a combined viability score for sensitivity. T47D Palbo-R cells displayed significantly higher Loewe synergy scores than T47D parental cells (**Fig. 4B**). In addition, T47D Palbo-R cells were also significantly more sensitive to the drug combination than T47D parental cells in terms of cellular viability (**Fig. 4C**). On the contrary, the WEE1 inhibitor AZD1775 and gemcitabine showed antagonism at most of the concentration combinations in both parental and Palbo-R T47D cells and displayed no significant difference in sensitivities between these two cell lines (Supplementary Fig. S12). In addition, 5-FU, the active metabolite of the nucleoside analog capecitabine that is commonly given orally to metastatic ER^+ breast cancer patients (63), also synergized with RP-6306 in T47D Palbo-R cells. T47D Palbo-R cells are also more sensitive to the 5-FU and RP-6306 combination compared to the parental line (Supplementary Fig. S13).

We further extended these observations to another set of ER^+ breast cancer cells, MCF7 and its EDR and EDR Palbo-R derivatives (20). MCF7 parental cells displayed very little synergy with the gemcitabine and RP-6306 combination and demonstrated similar viability as compared to MCF7 EDR and MCF7 EDR Palbo-R cells (Supplementary Fig. S14). Thus we focused on the comparison between MCF7 EDR and MCF7 EDR Palbo-R as another pair of palbociclib-sensitive and -resistant ER^+ cancer cell lines. Unlike T47D parental and T47D Palbo-R lines, the combination showed no synergy or greater sensitivity in viability in MCF7 EDR Palbo-R versus MCF7 EDR cells (**Fig. 4D** and **E**). A notable difference between T47D cells and MCF7 cells is that T47D cells harbor a loss-of-function L194F *TP53* mutation, whereas MCF7 cells are wild-type (WT) *TP53* (64, 65). p53 is a well-established transcription factor that acts as a tumor suppressor by guarding genome integrity by stopping the cell cycle in response to genotoxic stress (66). The effects of *TP53* knockdown in the MCF7 models were therefore tested using lentiviral transduction of two different shRNAs targeting *TP53* (Supplementary Fig. S15). Knocking down *TP53* selectively increased the synergy score for the drug combinations in MCF7 EDR Palbo-R cells but not in MCF7 EDR cells (**Fig. 4D**). Furthermore, knocking down *TP53* selectively increased the sensitivity to the drug combinations in MCF7 EDR Palbo-R cells but not in MCF7 EDR cells (**Fig. 4E**). In addition, we

(*Continued.*) T47D parental and Palbo-R cells, with and without 1 nmol/L gemcitabine cotreatment. **B** and **C,** Loewe synergy scores (**B**) and combination viability scores (**C**) of T47D parental and Palbo-R cells treated with different concentrations of RP-6306 and gemcitabine. **D** and **E,** Loewe synergy scores (**D**) and combination viability scores (**E**) of MCF7 EDR and MCF7 EDR Palbo-R cells stably transduced with lentiviruses expressing nontargeting shRNA (shNC) or two different *TP53*-targeting shRNAs, treated with different concentrations of RP-6306 and gemcitabine. In (**A**), curves and IC_{50}s were derived by the three-parameter log-logistic model. Vertical error bars show the standard errors of the mean of the viabilities. Horizontal error bars show the standard errors of the IC_{50}s. In (**B** and **D**), *P*-values were calculated by Wilcoxon signed-rank test, adjusted by the Holms method if more than one comparison was performed. The (arrows) display whether the value is higher or lower than the baseline. In (**C** and **E**), error bars show the SEM, the approximate *P*-values were calculated by *Z*-test using the SEM of the model, adjusted by the Holms method if more than one comparison was performed. In all experiments, data were analyzed from three independent biological replicates.

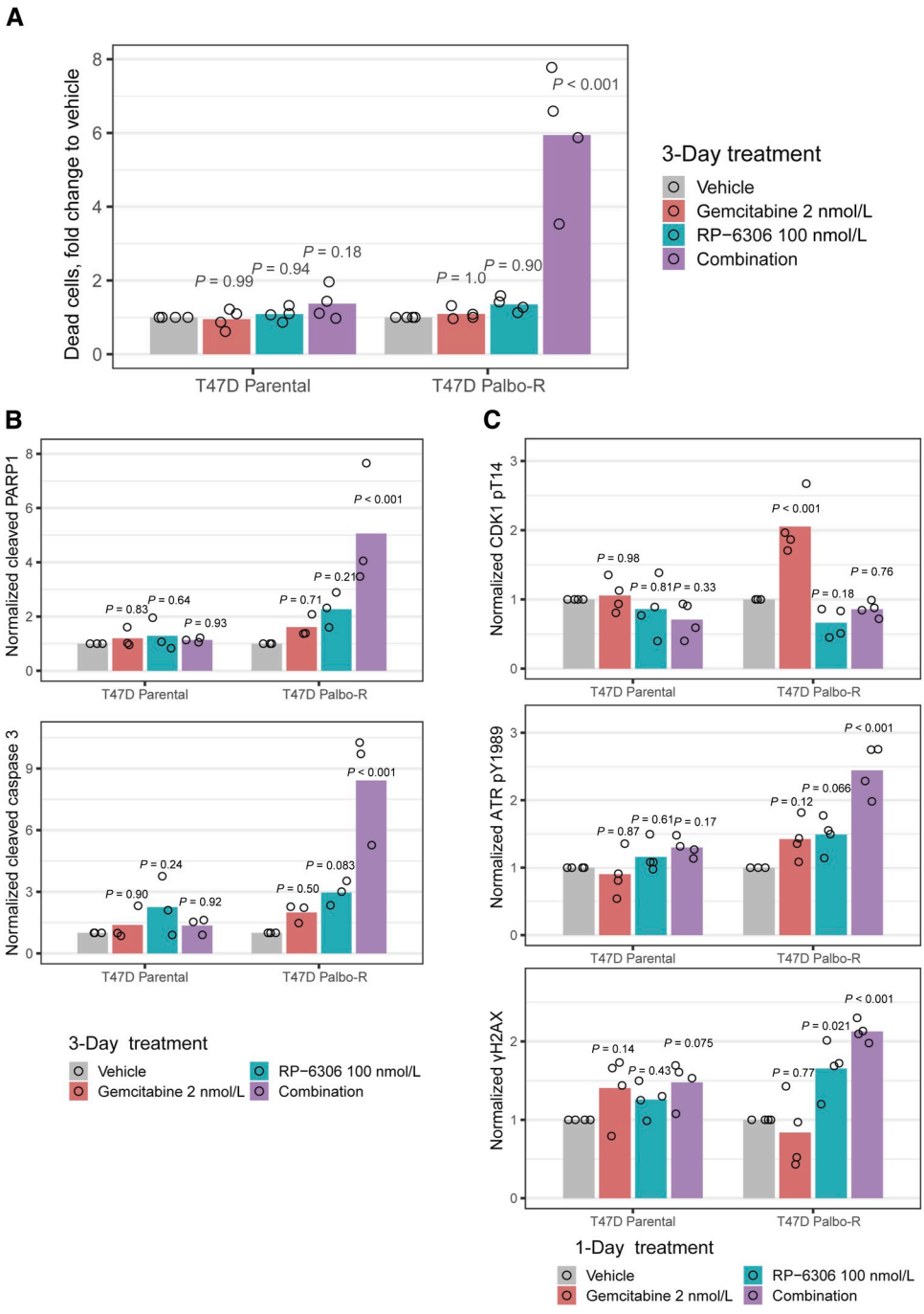

Figure 5.

The combination of RP-6306 and gemcitabine increases apoptosis and activates DNA damage signaling in palbociclib-resistant T47D cells. **A,** The relative abundance of dead cells after 3 days drug treatment, measured by a CellTox Green assay, is shown relative to the vehicle treatment. Bars show the means of individual biological repeats indicated by the dots. **B,** Quantification of immunoblotting of protein lysates made from cells treated with 100 nmol/L RP-6306 and/or 2 nmol/L gemcitabine for 3 days. Cleaved PARP1 and caspase 3 are known markers of apoptosis. GAPDH serves as a loading control. The figure is a representative image of three independent biological replicates. **C,** Quantification of immunoblotting of protein lysates made from cells treated with 100 nmol/L RP-6306 and/or 2 nmol/L gemcitabine for 1 day. PKMYT1 phosphorylation of CDK1 at pT14 was assayed. DNA damage was assayed by induction of phosphorylation of ATR (pY1989) and histone variant H2AX pS139 (also known as γH2AX). Total CDK1 and ATR serve as normalizing controls of the corresponding phosphorylated proteins, while GAPDH serves as a loading control. The figure is a representative image of four independent biological replicates. Supplementary Fig. S18 shows representative immunoblots for quantified data in (**B** and **C**). In all data panels, *P*-values were calculated by Dunnett's test (using the vehicle as the baseline) within each cell line.

tested the effect on the drug combination synergy and sensitivity when the L194F mutant p53 protein is "rescued" by WT p53 protein expression in T47D Palbo-R cells. To do this, we first knocked-down the L194F p53 using a lentiviral expressed shRNA targeting the 3′ untranslated region (3′ UTR) of the *p53* mRNA and then re-expressed a FLAG-tagged WT p53 (lacking the 3′ UTR) from a different lentiviral construct (Supplementary Fig. S16A). The presence of FLAG-tagged WT p53, whose turnover is rapid due to the 26S proteasome (67), was confirmed after cells were treated with the proteasome inhibitor, bortezomib. Knocking down the mutant p53 and re-expressing WT p53 in T47D Palbo-R cells reduced synergy with marginal significance ($P < 0.11$), but significantly reduced the sensitivity to the combination treatment (Supplementary Fig. S16B and S16C). In sum, the absence of functional p53 in the palbociclib-resistance setting contributes to the synergy and potency of the RP-6306 and gemcitabine combination.

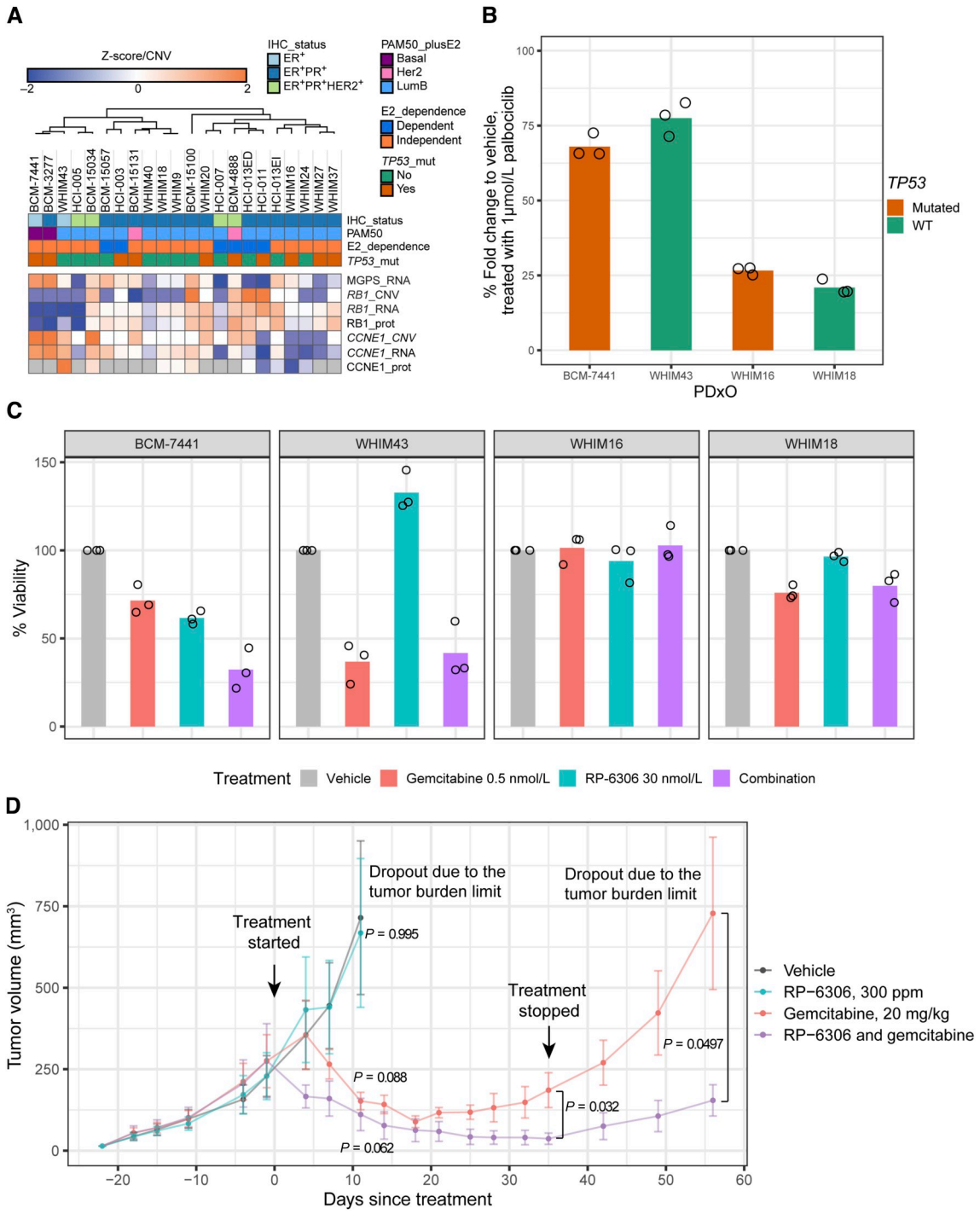

Figure 6.

The combination of RP-6306 and gemcitabine reduces the growth of *TP53*-mutant, palbociclib-resistant ER+ breast cancer PDX organoids (PDxO) and PDX tumors. **A,** Heatmap depicts the ERα IHC status, PAM50 gene expression, E2 dependence, *TP53* mutational status, an RNA-based MGPS, and RB1 and cyclin E1 copy number variation, mRNA, and protein levels in our collection of 22 ER+ breast cancer PDXs. PDXs were clustered by hierarchical clustering with one minus Pearson correlation. **B,** Two-week growth assay of four different PDxOs treated with 1 µmol/L palbociclib. Viability was assayed with a Cell Titer Glo 3D assay from three biological replicates. **C,** Two-week growth assay of four different PDxOs after treatment with vehicle, 0.5 nmol/L gemcitabine, 30 nmol/L RP-6306, or the combination of gemcitabine and RP-6306. In (**B** and **C**), bars show the means of three individual biological repeats indicated by the dots, and *P*-values of one-way ANOVA and Tukey HSD are reported in Supplementary Table S5. **D,** Tumor volumes of BCM-7441 PDX mice treated with vehicle ($n = 8$), RP-6306 ($n = 8$), gemcitabine ($n = 7$), and the combination of RP-6306 and gemcitabine ($n = 7$). Arrows indicate the start and the end of the 5-week treatment. Error bars reflect the standard errors of the mean. *P*-values were calculated by Dunnett's test (day 11, using the vehicle as the baseline) and *t* test (days 35 and 56, comparing the gemcitabine vs. combination groups).

The combination of RP-6306 and gemcitabine increases DNA damage and induces apoptosis in palbociclib-resistant, p53 loss-of-function cells

To determine if reduced cell viability in Palbo-R ER$^+$ breast cancer cells treated with gemcitabine and RP-6306 was due to an increase in cell death, T47D parental and T47D Palbo-R cell lines were treated with drug concentrations that yielded the highest synergy (2 nmol/L gemcitabine and 100 nmol/L RP-6306). Dead cells were labeled with "CellTox" Green dye and quantified at the mid-point of the previous viability assay treatment (3 days). In both T47D parental and Palbo-R cells, 2 nmol/L gemcitabine or 100 nmol/L RP-6306 as a single agent did not significantly increase the number of dead cells. However, the combination of gemcitabine and RP-6306 caused a significant 6-fold increase in the number of dead cells in the T47D Palbo-R line, but not in the T47D parental line (**Fig. 5A**; Supplementary Fig. S17).

To determine whether increased cell death was due to apoptosis, protein lysates from the T47D cell line experiment were prepared after 3 days of drug treatment to perform immunoblotting for two apoptosis markers, cleaved PARP1 (68) and cleaved caspase-3 (69). The combination treatment promoted the highest levels of these apoptosis markers in T47D Palbo-R (**Fig. 5B**; Supplementary Fig. S18A). To capture earlier molecular events, we characterized cell lysates after 1 day of treatment by immunoblotting. Importantly, 2 nmol/L of gemcitabine increased CDK1 pT14, a phospho-site whose only known kinase is PKMYT1 (13, 30, 39, 40), specifically in T47D Palbo-R cells, suggesting that gemcitabine induces PKMYT1 activity. As expected, CDK1 pT14 is repressed by the addition of RP-6306 (**Fig. 5C**; Supplementary Fig. S18B). These data support the conclusion that the PKMYT1-regulated G2/M checkpoint plays a critical role in ER$^+$ cells under replication stress induced by gemcitabine (70). When the gemcitabine-induced activation of PKMYT1 is reduced by RP-6306, the cells no longer adequately regulate the timing of the DNA damage repair and entry into mitosis, and a DNA damage signal is triggered [as assayed by γH2AX and ATR pY1989 (71, 72)] (**Fig. 5C**; Supplementary Fig. S18B), followed by apoptosis.

RP-6306 and gemcitabine reduce tumor growth in palbociclib-resistant, p53 mutant PDxOs and PDX tumors *in vivo*

The loss of RB1 and the upregulation of cyclin E1 (encoded by the *CCNE1* gene) are established molecular markers for CDK4/6i resistance in ER$^+$ breast cancer (56–59). To select preclinical therapeutic models, proteogenomic analysis of 22 ER$^+$ breast cancer PDXs was performed focused on *RB1*, *CCNE1*, an RNA-based MGPS (4) and *TP53* mutational status (**Fig. 6A**). Of the 22 PDX models, the E2-independent model, BCM-7441 was selected because of the presence of a missense loss-of-function *TP53* mutation in the DNA binding domain of p53 (R248Q) as well as membership in a cluster of PDX models with the lowest RB1 levels and highest cyclin E1 expression (**Fig. 6A**). Interestingly, although BCM-7441 is ER$^+$ based on IHC, it was classified as a basal-like subtype tumor by PAM50 profiling (38). In contrast, the E2-independent Luminal B PDX WHIM43 is a WT *TP53* model that is resistant to palbociclib (73), while the E2-independent Luminal B PDX WHIM16 is a *TP53* mutant (R116W) model sensitive to palbociclib. The Luminal B palbociclib-sensitive WHIM18 PDX is an E2-independent, WT *TP53* PDX model that is endocrine therapy-resistant due to expression of an ESR1-YAP1 fusion protein (22). We further confirmed palbociclib sensitivities of four above-mentioned models in PDX-derived organoids (PDxOs) treated with 1 μmol/L of palbociclib (**Fig. 6B**; *P*-values given in Supplementary Table S5). BCM-7441 PDxOs were subsequently treated with RP-6306 and gemcitabine at the single-agent concentration that gives an approximate 30% growth inhibition (0.5 nmol/L gemcitabine; 30 nmol/L RP-6306) in earlier cell line experiments. The combination of the two drugs significantly reduced viability compared to single-agent treatments (**Fig. 6C**; *P*-values given in Supplementary Table S5). In contrast, the effect of combination treatments on the three other PDxOs viability revealed no further reduction versus single agents (**Fig. 6C**). Both WHIM18 and WHIM16 PDxOs were much more resistant to RP-6306 than BCM-7441 PDxOs. WHIM43 demonstrated a strong response to single-agent gemcitabine, yet the effect of RP-6306 was minimal either as a single agent or as a combination treatment. Together, the results support the concept that the presence of a *TP53* mutation along with palbociclib resistance could be considered as a selection marker for a potential synergistic RP-6306 and gemcitabine combined treatment.

To confirm the palbociclib resistance of BCM-7441 *in vivo*, we treated BCM-7441 tumor-bearing mice with vehicle or palbociclib-containing chow at a dose that suppresses the growth of WHIM18 PDX tumors (70 mg/kg; ref. 22). BCM-7441 PDX tumors were indeed resistant to the palbociclib treatment (Supplementary Fig. S19A). We confirmed that palbociclib was adequately delivered to these mice, as palbociclib-treated mice displayed reduced RB1 phosphorylation in protein lysates made from liver tissue (Supplementary Fig. S19B).

To further validate the RP-6306 and gemcitabine combination sensitivity *in vivo*, BCM-7441 tumor-bearing mice were treated with vehicle control, 300 ppm of RP-6306 in chow, weekly intraperitoneal injection of 20 mg/kg gemcitabine, and the combination of RP-6306 and gemcitabine for 5 weeks (**Fig. 6D**). Little effect was observed in the RP-6306 treated group. On day 11, some mice in the vehicle group ($n = 2$) and RP-6306 treated group ($n = 3$) dropped out of the study due to tumors reaching maximum volume (1,500 mm^3). At this time point, a difference in tumor volume was observed between the vehicle group and the combination group at the margin of statistical significance ($P = 0.062$). As the treatment continued, both gemcitabine and the combination of RP-6306 and gemcitabine reduced the tumor volume, but the combination had a greater longer term effect on tumor size reduction. At the end of the 5-week treatment, the combination-treated tumors were significantly smaller than the gemcitabine-treated tumors. At the endpoint, blood was collected and RP-6306 circulating plasma levels were measured. We observed an average RP-6036–free plasma concentration of 54 nmol/L in the RP-6306–exposed animals (Supplementary Table S6), which was in the same concentration range required for achieving synergy with gemcitabine in cell lines and PDxOs. In the combination-treated group, five out of seven tumor sizes were reduced to a size too small to be measured by caliper (smaller than 3 mm in diameter), whereas none of the seven tumors in the gemcitabine group were reduced to that extent. The gemcitabine and the combination groups continued to be observed after treatment cessation, with combination-treated tumor regrowth lagging behind those treated with gemcitabine alone (**Fig. 6D**; Supplementary Fig. S19C). The animals in the combination treatment group experienced an approximate 10% body weight loss during the treatment period, however, the body weight recovered 1 week after treatment cessation (Supplementary Fig. S19D). Thus, our preclinical PDxO and PDX experiments validate the above cell line data and suggest that the RP-6306 and gemcitabine drug

combination warrants further clinical consideration for the treatment of ER+ breast cancers with *TP53* mutation and clinical CDK4/6 inhibitor and ET resistance.

Discussion

In this study, correlations between PKMYT1 mRNA and protein levels with poor prognosis, endocrine therapy, and CDK4/6i resistance in both clinical samples and in multiple preclinical models prompted experiments that demonstrated that PKMYT1 inhibition is a therapeutic vulnerability in ET and CDK4/6i resistant, *TP53* mutant ER+ breast cancer in combination with gemcitabine. Previously, Gallo and colleagues presented RP-6306 as a single treatment or a part of the combination treatment with gemcitabine for multiple cancer types with *CCNE1* amplification as a predictive biomarker (13), including HCC1569, an ER− HER2+ breast cancer cell line (74). However, the data described herein are distinct because of the specific focus on PKMYT1 in the ER+ HER2− setting.

Mechanistically, the importance of PKMYT1 in the regulation of the G2/M checkpoint in ER+ breast cancer cells has been understudied. Herein we demonstrate that the level of PKMYT1 in ER+ breast cancer is regulated by both ERα and E2F family members. While the E2F family plays critical roles in essentially all cancer types, the regulation of PKMYT1 by ERα suggests a specific functional role in the ER+ breast cancer cell cycle. E2 has been reported to induce DNA replication stress (75, 76), which may be mutagenic, likely demanding an additional G2/M checkpoint control beyond that provided by WEE1. In addition, there is a PKMYT1-regulated phosphorylation site in CDK1 that is not regulated by WEE1, suggesting a specific, albeit underexplored PKMYT1-dependent regulatory step at G2/M in ER+ breast cancer cells. As p53 regulates all stages of the cell cycle (77), the absence of functional p53 causes a dysregulated cell cycle and poor clinical outcomes in ER+ breast cancer (78, 79). Here we show that the loss of p53 in CDK4/6i-resistant breast cancer causes tumor cells to be more vulnerable to PKMYT1 inhibition. Together, PKMYT1 is a selective vulnerability in ER+ breast tumors with absent functional p53 and in the presence of CDK4/6i resistance. Importantly, WEE1 inhibition in combination with chemotherapy is toxic, with clinical trials often terminated because of grade 4 and 5 events (80, 81). Given that PKMYT1 is E2-regulated in ER+ lineages, unlike WEE1, this setting may represent a cleaner setting from the therapeutic ratio perspective.

In terms of the populations in whom PKMYT1 inhibition should be considered, the T47D and MCF7 data herein suggest that cyclin E overexpression may not be the only predictive biomarker for the efficacy of RP-6306 and gemcitabine combination (13). T47D Palbo-R cells' response suggests that CDK4/6i resistance that is not mediated by cyclin E overexpression can also expose vulnerability to PKMYT1 inhibition and gemcitabine. MCF7 data suggest that mutant *TP53* status should also be taken into consideration as an eligibility or stratification factor. Although *TP53* alterations are less common in primary ER+ breast tumors compared to other breast cancer subtypes, they are enriched in CDK4/6i-resistant metastatic ER+ breast cancer (57, 82), with a frequency up to 58.5% (57). While the enrollment of patients with advanced disease treatment will be the necessary first step in explorations of gemcitabine (or potentially capecitabine given our cell line 5-FU data) and PKMYT1 inhibition in ER+ breast cancer, neoadjuvant data with anastrozole and palbociclib illustrated herein suggest that there is also a poor prognosis early-stage population that could be targeted with this treatment. In this setting, eligible cases could be identified through *TP53* mutation and evidence for functional ET- and CDK4/6i-resistance based on persistent Ki67 expression despite treatment.

While the focus of this study was to address whether PKMYT1 may represent a response marker for CDK4/6i response and a therapeutic strategy in combination with gemcitabine for CDK4/6i resistance in ER+ breast cancer, the finding that RP-6306 and gemcitabine combination is effective against CDK4/6i-resistance with *TP53* mutation infers that this combination may also be effective in other breast cancer subtypes displaying similar characteristics. Namely, TNBC tumors often display low RB1 and high Cyclin E1, with *TP53* loss-of-function mutations (83). Consistent with this hypothesis, two groups have reported that, in TNBC patients, high expression of PKMYT1 correlates with poor prognosis (37, 84). Furthermore, the knockdown of *PKMYT1* in TNBC lines revealed a significant reduction in cell proliferation, colony formation, cell migration and cell invasion, epithelial–mesenchymal transition, and Notch signaling, with an increase in apoptosis (84, 85). Future studies are clearly needed to test the efficacy of PKMYT1 inhibition in reducing the growth of TNBC tumors with *TP53* mutations and G1/S checkpoint dysregulation by mechanisms such as cyclin E1 overexpression.

In conclusion, this study illustrates the expanding toolbox of techniques that can be deployed to identify novel approaches to treatment-resistant ER+ breast cancer. These include proteogenomic analysis, targeted proteomic techniques focused on therapeutic target discovery including KIPA, and samples from neoadjuvant ET and CDK4/6i treatments to expose resistance patterns and mechanisms. An expanding set of ER+ PDX models that reflect the extreme diversity of clinical phenotypes and genotypes in ER+ breast cancer is also proving increasingly useful. The combined and integrated use of these tools to successfully expose new therapeutic liabilities is illustrated by the PKMYT1 findings outlined herein.

Authors' Disclosures

A. Chen reports grants from Repare Therapeutics during the conduct of the study; other support from Repare Therapeutics outside the submitted work. M.P. Goetz reports other support from ARC Therapuetics, Biotheranostics, Biotheryx, Blueprint Medicines, Engage Health Media, Laekna, Novartis, RNA Diagnostics, Seattle Genetics, and TerSera Therapeutics; grants and other support from AstraZeneca, Lilly, and Sermonix; grants from ATOSSA Therapeutics, Loxo, and Pfizer; personal fees from Research to Practice, Medscape, MJH Life Sciences, and Total Health Conferencing; personal fees from Curio Science outside the submitted work. S.G. Hilsenbeck reports grants from NIH during the conduct of the study. C.G. Marshall reports other support from Repare Therapeutics outside the submitted work. M.L. Hyer reports other support from Repare Therapeutics during the conduct of the study. R. Papp reports other support from Repare Therapeutics Inc. outside the submitted work. S.-Y. Yin reports other support from Repare Therapeutics Inc. outside the submitted work. R. Schiff reports grants from Breast Cancer Research Foundation during the conduct of the study; grants from Gilead Sciences, Puma, Biotechnology Inc., Seagen, and AstraZeneca; personal fees from Daiichi Sankyo, MacroGenics, and Binaytara Foundation; other support from Dava Oncology, LP; personal fees from UpToDate outside the submitted work; in addition, R. Schiff has a patent for PCT/US21/70543 (Methods for breast cancer treatment and prediction of therapeutic response) pending; and UTSA/SABCS—Personal Fees/travel support as a participated faculty. C.X. Ma reports grants from Pfizer during the conduct of the study; personal fees from Danatlas, Rigor Therapeutics, Merck, Loxo, Novartis, Daiichi, Stemline, Pfizer, AstraZeneca, Olaris, and TerSera; personal fees from Sanofi outside the submitted work. C.E. Foulds reports other support from Repare Therapeutics and Golfers Against Cancer during the conduct of the study; equity positions in CoActigon, Inc. and CoRegen, Inc. outside the submitted work; in addition, C.E. Foulds has a patent for PCT/US2022/077924 pending. M.J. Ellis reports he was employed by AstraZeneca

between 3/22 and 3/24. AstraZeneca was not involved in the submitted work. No disclosures were reported by the other authors.

Authors' Contributions

A. Chen: Conceptualization, data curation, software, formal analysis, validation, investigation, visualization, methodology, writing—original draft. **B.-J. Kim:** Data curation, formal analysis, validation, investigation, methodology. **A. Mitra:** Formal analysis, investigation, methodology. **C.T. Vollert:** Formal analysis, investigation, methodology. **J.T. Lei:** Data curation, software, formal analysis. **D. Fandino:** Investigation. **M. Anurag:** Data curation, software, formal analysis. **M.V. Holt:** Investigation, methodology. **X. Gou:** Investigation, methodology. **J.B. Pilcher:** Investigation. **M.P. Goetz:** Resources, data curation. **D.W. Northfelt:** Resources, data curation. **S.G. Hilsenbeck:** Software, formal analysis. **C.G. Marshall:** Resources, formal analysis. **M.L. Hyer:** Resources, formal analysis. **R. Papp:** Investigation, methodology. **S.-Y. Yin:** Investigation, methodology. **C. De Angelis:** Resources. **R. Schiff:** Resources, formal analysis, writing—review and editing. **S.A.W. Fuqua:** Resources, formal analysis, writing—review and editing. **C.X. Ma:** Conceptualization, resources, data curation, formal analysis, methodology. **C.E. Foulds:** Conceptualization, resources, supervision, funding acquisition, project administration, writing—review and editing. **M.J. Ellis:** Conceptualization, resources, supervision, funding acquisition, project administration, writing—review and editing.

Acknowledgments

We gratefully acknowledge Drs. Xiang Zhang, Xi Chen, Bing Zhang, Bora Lim, Eric C. Chang, and Meghashyam Kavuri at BCM for their scientific input, and Dr. Alana L. Welm at the University of Utah, Dr. Shunqiang Li at Washington University, and Dr. Michael T. Lewis at BCM for previously developing HCI, WHIM, and BCM ER$^+$ PDX models, respectively. This work was supported by the following grants to M.J. Ellis from the Susan G. Komen Foundation (SAC190059, which supported M. Anurag, M.J. Ellis, X. Gou, and A. Chen; PG12220321, which supported J.T. Lei, M.J. Ellis, and X. Gou), and National Cancer Institute Grants P50CA186784, which supported B.-J. Kim, J.T. Lei, M. Anurag, M.J. Ellis, S.G. Hilsenbeck, and R. Schiff; U54CA233223, which supported D. Fandino, C.T. Vollert, M. Anurag, B.-J. Kim, J.B. Pilcher, M.J. Ellis, A. Chen, and C.E. Foulds; and U01CA214125, which supported M.V. Holt, B.-J. Kim, C.T. Vollert, M. Anurag, M.J. Ellis, and S.G. Hilsenbeck. M.J. Ellis was a Susan G. Komen Foundation Scholar, a McNair Scholar supported by the McNair Medical Institute at The Robert and Janice McNair Foundation, and a recipient of a Cancer Prevention and Research Institute of Texas (CPRIT) Established Investigator Award (RR140033, which supported X. Gou, J.T. Lei, M. Anurag, D. Fandino, and B.-J. Kim). This work was supported by funding to C.E. Foulds: a SPORE Developmental Research Project grant (supported by P50CA186784, which supported A. Chen and C.E. Foulds), a SRA with Repare Therapeutics, which supported A. Chen and C.E. Foulds, and a charitable gift from Golfers Against Cancer, which supported A. Chen and C.E. Foulds. S.A.W. Fuqua acknowledges support from NIH R01CA072038 and Breast Cancer Research Foundation BCRF 22-055. This work was also partly supported by the Breast Cancer Research Foundation BCRF 20-145, 21-145, 22-145, 23-145 to R. Schiff. C. De Angelis was supported in part by CPRIT RP140102. X. Gou was also supported by a CPRIT training grant RP210027. J.T. Lei was also supported by a NIH training grant T32CA203690. A. Mitra was supported by CPRIT RP220050. PDX mice work was also supported by U54CA224076 to M.T. Lewis and A.L. Welm and U54CA224083 to S. Li. The BCM ER$^+$ PDX was generated with a CPRIT Core Facility Support Grant to CPRIT Scholar M.T. Lewis (RP170691) and P30 Cancer Center Support Grant (P30CA125123). We gratefully acknowledge Pfizer for funding the NeoPalAna clinical trial.

Note

Supplementary data for this article are available at Molecular Cancer Therapeutics Online (http://mct.aacrjournals.org/).

Received August 26, 2023; revised March 25, 2024; accepted May 14, 2024; published first May 23, 2024.

References

1. Narod SA, Giannakeas V, Sopik V. Time to death in breast cancer patients as an indicator of treatment response. Breast Cancer Res Treat 2018;172:659–69.
2. Shah M, Nunes MR, Stearns V. CDK4/6 inhibitors: game changers in the management of hormone receptor-positive advanced breast cancer? Oncology (Williston Park) 2018;32:216–22.
3. Ellis MJ. Lessons in precision oncology from neoadjuvant endocrine therapy trials in ER$^+$ breast cancer. Breast 2017;34(Suppl 1):S104–S7.
4. Ellis MJ, Suman VJ, Hoog J, Goncalves R, Sanati S, Creighton CJ, et al. Ki67 proliferation index as a tool for chemotherapy decisions during and after neoadjuvant aromatase inhibitor treatment of breast cancer: results from the American College of Surgeons Oncology Group Z1031 Trial (Alliance). J Clin Oncol 2017;35:1061–9.
5. Modi S, Jacot W, Yamashita T, Sohn J, Vidal M, Tokunaga E, et al. Trastuzumab deruxtecan in previously treated HER2-low advanced breast cancer. N Engl J Med 2022;387:9–20.
6. Early Breast Cancer Trialists' Collaborative Group EBCTCG; Peto R, Davies C, Godwin J, Gray R, Pan HC, et al. Comparisons between different polychemotherapy regimens for early breast cancer: meta-analyses of long-term outcome among 100,000 women in 123 randomised trials. Lancet 2012;379:432–44.
7. Duong-Ly KC, Peterson JR. The human kinome and kinase inhibition. Curr Protoc Pharmacol 2013;Chapter 2:Unit2.9.
8. Bhullar KS, Lagarón NO, McGowan EM, Parmar I, Jha A, Hubbard BP, et al. Kinase-targeted cancer therapies: progress, challenges and future directions. Mol Cancer 2018;17:48.
9. Gou X, Kim BJ, Anurag M, Lei JT, Young MN, Holt MV, et al. Kinome reprogramming is a targetable vulnerability in ESR1 fusion-driven breast cancer. Cancer Res 2023;83:3237–51.
10. Wang J, Saltzman AB, Jaehnig EJ, Lei JT, Malovannaya A, Holt MV, et al. Kinase inhibitor pulldown assay identifies a chemotherapy response signature in triple-negative breast cancer based on purine-binding proteins. Cancer Res Commun 2023;3:1551–63.
11. Saltzman AB, Chan DW, Holt MV, Wang J, Jaehnig EJ, Anurag M, et al. Kinase inhibitor pulldown assay (KiP) for clinical proteomics. Clin Proteomics 2024;21:3.
12. East MP, Johnson GL. Adaptive chromatin remodeling and transcriptional changes of the functional kinome in tumor cells in response to targeted kinase inhibition. J Biol Chem 2022;298:101525.
13. Gallo D, Young JTF, Fourtounis J, Martino G, Álvarez-Quilón A, Bernier C, et al. CCNE1 amplification is synthetic lethal with PKMYT1 kinase inhibition. Nature 2022;604:749–56.
14. Pereira B, Chin S-F, Rueda OM, Vollan H-KM, Provenzano E, Bardwell HA, et al. The somatic mutation profiles of 2,433 breast cancers refines their genomic and transcriptomic landscapes. Nat Commun 2016;7:11479.
15. Curtis C, Shah SP, Chin SF, Turashvili G, Rueda OM, Dunning MJ, et al. The genomic and transcriptomic architecture of 2,000 breast tumours reveals novel subgroups. Nature 2012;486:346–52.
16. Krug K, Jaehnig EJ, Satpathy S, Blumenberg L, Karpova A, Anurag M, et al. Proteogenomic landscape of breast cancer tumorigenesis and targeted therapy. Cell 2020;183:1436–56.e31.
17. Ma CX, Gao F, Luo J, Northfelt DW, Goetz M, Forero A, et al. NeoPalAna: neoadjuvant palbociclib, a cyclin-dependent kinase 4/6 inhibitor, and anastrozole for clinical stage 2 or 3 estrogen receptor-positive breast cancer. Clin Cancer Res 2017;23:4055–65.
18. Whitfield ML, Sherlock G, Saldanha AJ, Murray JI, Ball CA, Alexander KE, et al. Identification of genes periodically expressed in the human cell cycle and their expression in tumors. Mol Biol Cell 2002;13:1977–2000.
19. Dustin D, Gu G, Beyer AR, Herzog SK, Edwards DG, Lin H, et al. RON signalling promotes therapeutic resistance in ESR1 mutant breast cancer. Br J Cancer 2021;124:191–206.
20. De Angelis C, Fu X, Cataldo ML, Nardone A, Pereira R, Veeraraghavan J, et al. Activation of the IFN signaling pathway is associated with resistance to CDK4/6 inhibitors and immune checkpoint activation in ER-positive breast cancer. Clin Cancer Res 2021;27:4870–82.

21. Szychowski J, Papp R, Dietrich E, Liu B, Vallée F, Leclaire M-E, et al. Discovery of an orally bioavailable and selective PKMYT1 inhibitor, RP-6306. J Med Chem 2022;65:10251–84.
22. Lei JT, Shao J, Zhang J, Iglesia M, Chan DW, Cao J, et al. Functional annotation of ESR1 gene fusions in estrogen receptor-positive breast cancer. Cell Rep 2018;24:1434–44.e7.
23. Schneider CA, Rasband WS, Eliceiri KW. NIH image to imageJ: 25 years of image analysis. Nat Methods 2012;9:671–5.
24. Zheng S, Wang W, Aldahdooh J, Malyutina A, Shadbahr T, Tanoli Z, et al. SynergyFinder plus: toward better interpretation and annotation of drug combination screening datasets. Genomics Proteomics Bioinformatics 2022; 20:587–96.
25. Ritz C, Baty F, Streibig JC, Gerhard D. Dose-response analysis using R. PLoS One 2015;10:e0146021.
26. Perez-Riverol Y, Bai J, Bandla C, García-Seisdedos D, Hewapathirana S, Kamatchinathan S, et al. The PRIDE database resources in 2022: a hub for mass spectrometry-based proteomics evidences. Nucleic Acids Res 2022;50: D543–52.
27. Gou X, Anurag M, Lei JT, Kim BJ, Singh P, Seker S, et al. Transcriptional reprogramming differentiates active from inactive ESR1 fusions in endocrine therapy-refractory metastatic breast cancer. Cancer Res 2021;81:6259–72.
28. Booher RN, Holman PS, Fattaey A. Human Myt1 is a cell cycle-regulated kinase that inhibits Cdc2 but not Cdk2 activity. J Biol Chem 1997;272:22300–6.
29. Ghelli Luserna di Rorà A, Cerchione C, Martinelli G, Simonetti G. A WEE1 family business: regulation of mitosis, cancer progression, and therapeutic target. J Hematol Oncol 2020;13:126.
30. Mueller PR, Coleman TR, Kumagai A, Dunphy WG. Myt1: a membrane-associated inhibitory kinase that phosphorylates Cdc2 on both threonine-14 and tyrosine-15. Science 1995;270:86–90.
31. Zheng R, Wan C, Mei S, Qin Q, Wu Q, Sun H, et al. Cistrome data browser: expanded datasets and new tools for gene regulatory analysis. Nucleic Acids Res 2019;47:D729–35.
32. Gates LA, Foulds CE, O'Malley BW. Histone marks in the 'driver's seat': functional roles in steering the transcription cycle. Trends Biochem Sci 2017; 42:977–89.
33. Ochsner SA, Abraham D, Martin K, Ding W, McOwiti A, Kankanamge W, et al. The signaling pathways project, an integrated [L8S2Q1M6]omics knowledgebase for mammalian cellular signaling pathways. Sci Data 2019;6: 252.
34. Osborne CK, Wakeling A, Nicholson RI. Fulvestrant: an oestrogen receptor antagonist with a novel mechanism of action. Br J Cancer 2004;90(Suppl 1): S2–6.
35. Stack G, Kumar V, Green S, Ponglikitmongkol M, Berry M, Rio MC, et al. Structure and function of the pS2 gene and estrogen receptor in human breast cancer cells. Cancer Treat Res 1988;40:185–206.
36. Zhu W, Giangrande PH, Nevins JR. E2Fs link the control of G1/S and G2/M transcription. EMBO J 2004;23:4615–26.
37. Liu Y, Qi J, Dou Z, Hu J, Lu L, Dai H, et al. Systematic expression analysis of WEE family kinases reveals the importance of PKMYT1 in breast carcinogenesis. Cell Prolif 2020;53:e12741.
38. Nielsen TO, Parker JS, Leung S, Voduc D, Ebbert M, Vickery T, et al. A comparison of PAM50 intrinsic subtyping with immunohistochemistry and clinical prognostic factors in tamoxifen-treated estrogen receptor-positive breast cancer. Clin Cancer Res 2010;16:5222–32.
39. Chow JP, Poon RY. The CDK1 inhibitory kinase MYT1 in DNA damage checkpoint recovery. Oncogene 2013;32:4778–88.
40. Liu F, Stanton JJ, Wu Z, Piwnica-Worms H. The human Myt1 kinase preferentially phosphorylates Cdc2 on threonine 14 and localizes to the endoplasmic reticulum and golgi complex. Mol Cell Biol 1997;17:571–83.
41. Liberzon A, Birger C, Thorvaldsdóttir H, Ghandi M, Mesirov JP, Tamayo P. The Molecular Signatures Database (MSigDB) hallmark gene set collection. Cell Syst 2015;1:417–25.
42. Hiebert SW, Chellappan SP, Horowitz JM, Nevins JR. The interaction of RB with E2F coincides with an inhibition of the transcriptional activity of E2F. Genes Dev 1992;6:177–85.
43. Goel S, DeCristo MJ, McAllister SS, Zhao JJ. CDK4/6 inhibition in cancer: beyond cell cycle arrest. Trends Cell Biol 2018;28:911–25.
44. Sabbah M, Courilleau D, Mester J, Redeuilh G. Estrogen induction of the cyclin D1 promoter: involvement of a cAMP response-like element. Proc Natl Acad Sci U S A 1999;96:11217–22.
45. Turner NC, Slamon DJ, Ro J, Bondarenko I, Im SA, Masuda N, et al. Overall survival with palbociclib and fulvestrant in advanced breast cancer. N Engl J Med 2018;379:1926–36.
46. Sledge GW Jr, Toi M, Neven P, Sohn J, Inoue K, Pivot X, et al. Monarch 2: abemaciclib in combination with fulvestrant in women with HR$^+$/HER2$^-$ advanced breast cancer who had progressed while receiving endocrine therapy. J Clin Oncol 2017;35:2875–84.
47. Tripathy D, Im SA, Colleoni M, Franke F, Bardia A, Harbeck N, et al. Ribociclib plus endocrine therapy for premenopausal women with hormone-receptor-positive, advanced breast cancer (MONALEESA-7): a randomised phase 3 trial. Lancet Oncol 2018;19:904–15.
48. Finn RS, Martin M, Rugo HS, Jones S, Im SA, Gelmon K, et al. Palbociclib and letrozole in advanced breast cancer. N Engl J Med 2016;375:1925–36.
49. Yang C, Li Z, Bhatt T, Dickler M, Giri D, Scaltriti M, et al. Acquired CDK6 amplification promotes breast cancer resistance to CDK4/6 inhibitors and loss of ER signaling and dependence. Oncogene 2017;36:2255–64.
50. Li Q, Jiang B, Guo J, Shao H, Del Priore IS, Chang Q, et al. INK4 tumor suppressor proteins mediate resistance to CDK4/6 kinase inhibitors. Cancer Discov 2022;12:356–71.
51. Cao AR, Rabinovich R, Xu M, Xu X, Jin VX, Farnham PJ. Genome-wide analysis of transcription factor E2F1 mutant proteins reveals that N- and C-terminal protein interaction domains do not participate in targeting E2F1 to the human genome. J Biol Chem 2011;286:11985–96.
52. Mohammed H, D'Santos C, Serandour AA, Ali HR, Brown GD, Atkins A, et al. Endogenous purification reveals GREB1 as a key estrogen receptor regulatory factor. Cell Rep 2013;3:342–9.
53. Yan Z, DeGregori J, Shohet R, Leone G, Stillman B, Nevins JR, et al. Cdc6 is regulated by E2F and is essential for DNA replication in mammalian cells. Proc Natl Acad Sci U S A 1998;95:3603–8.
54. Zhou X, Sumazin P, Rajbhandari P, Califano A. A systems biology approach to transcription factor binding site prediction. PLoS One 2010;5:e9878.
55. Finn RS, Dering J, Conklin D, Kalous O, Cohen DJ, Desai AJ, et al. PD 0332991, a selective cyclin D kinase 4/6 inhibitor, preferentially inhibits proliferation of luminal estrogen receptor-positive human breast cancer cell lines *in vitro*. Breast Cancer Res 2009;11:R77.
56. Condorelli R, Spring L, O'Shaughnessy J, Lacroix L, Bailleux C, Scott V, et al. Polyclonal RB1 mutations and acquired resistance to CDK 4/6 inhibitors in patients with metastatic breast cancer. Ann Oncol 2018;29:640–5.
57. Wander SA, Cohen O, Gong X, Johnson GN, Buendia-Buendia JE, Lloyd MR, et al. The genomic landscape of intrinsic and acquired resistance to cyclin-dependent kinase 4/6 inhibitors in patients with hormone receptor-positive metastatic breast cancer. Cancer Discov 2020;10:1174–93.
58. Turner NC, Liu Y, Zhu Z, Loi S, Colleoni M, Loibl S, et al. Cyclin E1 expression and palbociclib efficacy in previously treated hormone receptor-positive metastatic breast cancer. J Clin Oncol 2019;37:1169–78.
59. Guarducci C, Bonechi M, Benelli M, Biagioni C, Boccalini G, Romagnoli D, et al. Cyclin E1 and Rb modulation as common events at time of resistance to palbociclib in hormone receptor-positive breast cancer. NPJ Breast Cancer 2018;4:38.
60. O'Connor MJ. Targeting the DNA damage response in cancer. Mol Cell 2015; 60:547–60.
61. Hirai H, Iwasawa Y, Okada M, Arai T, Nishibata T, Kobayashi M, et al. Small-molecule inhibition of Wee1 kinase by MK-1775 selectively sensitizes p53-deficient tumor cells to DNA-damaging agents. Mol Cancer Ther 2009;8: 2992–3000.
62. Huppert LA, Gumusay O, Idossa D, Rugo HS. Systemic therapy for hormone receptor-positive/human epidermal growth factor receptor 2-negative early stage and metastatic breast cancer. CA Cancer J Clin 2023;73:480–515.
63. Alvarado-Miranda A, Lara-Medina FU, Muñoz-Montano WR, Zinser-Sierra JW, Galeana PAC, Garza CV, et al. Capecitabine plus aromatase inhibitor as first line therapy for hormone receptor positive, HER2 negative metastatic breast cancer. Curr Oncol 2023;30:6097–110.
64. Nigro JM, Baker SJ, Preisinger AC, Jessup JM, Hostetter R, Cleary K, et al. Mutations in the p53 gene occur in diverse human tumour types. Nature 1989; 342:705–8.
65. Kao J, Salari K, Bocanegra M, Choi YL, Girard L, Gandhi J, et al. Molecular profiling of breast cancer cell lines defines relevant tumor models and provides a resource for cancer gene discovery. PLoS One 2009;4:e6146.
66. Marei HE, Althani A, Afifi N, Hasan A, Caceci T, Pozzoli G, et al. p53 signaling in cancer progression and therapy. Cancer Cell Int 2021;21:703.

67. Maki CG, Huibregtse JM, Howley PM. *In vivo* ubiquitination and proteasome-mediated degradation of p53(1). Cancer Res 1996;56:2649–54.
68. Tewari M, Quan LT, O'Rourke K, Desnoyers S, Zeng Z, Beidler DR, et al. Yama/CPP32 beta, a mammalian homolog of CED-3, is a CrmA-inhibitable protease that cleaves the death substrate poly(ADP-ribose) polymerase. Cell 1995;81:801–9.
69. McIlwain DR, Berger T, Mak TW. Caspase functions in cell death and disease. Cold Spring Harb Perspect Biol 2013;5:a008656.
70. Forment JV, O'Connor MJ. Targeting the replication stress response in cancer. Pharmacol Ther 2018;188:155–67.
71. Mah LJ, El-Osta A, Karagiannis TC. gammaH2AX: a sensitive molecular marker of DNA damage and repair. Leukemia 2010;24:679–86.
72. Nam EA, Zhao R, Glick GG, Bansbach CE, Friedman DB, Cortez D. Thr-1989 phosphorylation is a marker of active ataxia telangiectasia-mutated and Rad3-related (ATR) kinase. J Biol Chem 2011;286:28707–14.
73. Wardell SE, Ellis MJ, Alley HM, Eisele K, VanArsdale T, Dann SG, et al. Efficacy of SERD/SERM hybrid-CDK4/6 inhibitor combinations in models of endocrine therapy-resistant breast cancer. Clin Cancer Res 2015;21:5121–30.
74. Riaz M, van Jaarsveld MTM, Hollestelle A, Prager-van der Smissen WJC, Heine AAJ, Boersma AWM, et al. miRNA expression profiling of 51 human breast cancer cell lines reveals subtype and driver mutation-specific miRNAs. Breast Cancer Res 2013;15:R33.
75. Stork CT, Bocek M, Crossley MP, Sollier J, Sanz LA, Chedin F, et al. Co-transcriptional R-loops are the main cause of estrogen-induced DNA damage. Elife 2016;5:e17548.
76. Caldon CE. Estrogen signaling and the DNA damage response in hormone dependent breast cancers. Front Oncol 2014;4:106.
77. Rizzotto D, Englmaier L, Villunger A. At a crossroads to cancer: how p53-induced cell fate decisions secure genome integrity. Int J Mol Sci 2021;22:10883.
78. Meric-Bernstam F, Zheng X, Shariati M, Damodaran S, Wathoo C, Brusco L, et al. Survival outcomes by *TP53* mutation status in metastatic breast cancer. JCO Precis Oncol 2018;2018:PO.17.00245.
79. Ungerleider NA, Rao SG, Shahbandi A, Yee D, Niu T, Frey WD, et al. Breast cancer survival predicted by TP53 mutation status differs markedly depending on treatment. Breast Cancer Res 2018;20:115.
80. Leijen S, van Geel RMJM, Pavlick AC, Tibes R, Rosen L, Razak ARA, et al. Phase I study evaluating WEE1 inhibitor AZD1775 as monotherapy and in combination with gemcitabine, cisplatin, or carboplatin in patients with advanced solid tumors. J Clin Oncol 2016;34:4371–80.
81. Kato H, de Souza P, Kim SW, Lickliter JD, Naito Y, Park K, et al. Safety, pharmacokinetics, and clinical activity of adavosertib in combination with chemotherapy in Asian patients with advanced solid tumors: phase Ib study. Target Oncol 2020;15:75–84.
82. Park YH, Im SA, Park K, Wen J, Lee KH, Choi YL, et al. Longitudinal multi-omics study of palbociclib resistance in HR-positive/HER2-negative metastatic breast cancer. Genome Med 2023;15:55.
83. Sporikova Z, Koudelakova V, Trojanec R, Hajduch M. Genetic markers in triple-negative breast cancer. Clin Breast Cancer 2018;18:e841–50.
84. Li H, Wang L, Zhang W, Dong Y, Cai Y, Huang X, et al. Overexpression of PKMYT1 associated with poor prognosis and immune infiltration may serve as a target in triple-negative breast cancer. Front Oncol 2022;12:1002186.
85. Li B, Huang L, Ruan J. PKMYT1 promotes epithelial-mesenchymal transition process in triple-negative breast cancer by activating Notch signaling. Rev Invest Clin 2024;76:45–59.